JCB Journal of Cell Biology

ARTICLE

Expanded directly binds conserved regions of Fat to restrain growth via the Hippo pathway

Alexander D. Fulford[1], Leonie Enderle[2], Jannette Rusch[1], Didier Hodzic[1], Maxine V. Holder[3], Alex Earl[1], Robin Hyunseo Oh[2], Nicolas Tapon[3], and Helen McNeill[1,2]

The Hippo pathway is a conserved and critical regulator of tissue growth. The FERM protein Expanded is a key signaling hub that promotes activation of the Hippo pathway, thereby inhibiting the transcriptional co-activator Yorkie. Previous work identified the polarity determinant Crumbs as a primary regulator of Expanded. Here, we show that the giant cadherin Fat also regulates Expanded directly and independently of Crumbs. We show that direct binding between Expanded and a highly conserved region of the Fat cytoplasmic domain recruits Expanded to the apicolateral junctional zone and stabilizes Expanded. In vivo deletion of Expanded binding regions in Fat causes loss of apical Expanded and promotes tissue overgrowth. Unexpectedly, we find Fat can bind its ligand Dachsous via interactions of their cytoplasmic domains, in addition to the known extracellular interactions. Importantly, Expanded is stabilized by Fat independently of Dachsous binding. These data provide new mechanistic insights into how Fat regulates Expanded, and how Hippo signaling is regulated during organ growth.

Introduction

The precise and coordinated control of metazoan growth is essential for correctly sized and proportioned adult organisms, and the highly conserved Hippo pathway is key to its regulation. The Hippo pathway modulates growth by inhibiting the transcriptional co-activator Yorkie (Yki). Yki activity is controlled by the core Hippo kinase cassette consisting of the kinases Hippo (Hpo; Harvey et al., 2003; Jia et al., 2003; Pantalacci et al., 2003; Udan et al., 2003; Wu et al., 2003) and Warts (Wts; Justice et al., 1995; Xu et al., 1995), which phosphorylates Yki and inhibits its nuclear localization (Huang et al., 2005). When free from inhibition by these kinases, Yki concentrates in the nucleus where it interacts with transcription factors such as Scalloped to promote transcription of cell cycle and anti-apoptotic genes, for example, *cyclinE* and *diap1*, ultimately driving tissue growth (Wu et al., 2008; Zhang et al., 2008). Once Yki is activated, excessive growth is prevented through a negative feedback loop, whereby Yki drives the transcription of its own inhibitors, such as *expanded* (*ex*; Fulford et al., 2018; Zheng and Pan, 2019).

Upstream of the kinase cassette are numerous inputs into the pathway, such as cell polarity, adherens junctions, and the cytoskeleton (Fulford et al., 2018; Zheng and Pan, 2019). One important nexus of signaling is through the 4.1, Ezrin, Radixin, and Moesin (FERM) protein Ex. Ex forms a complex with Merlin (Mer) and Kibra at the apical junctions (termed the KEM complex), where Ex activates the Hippo kinase cassette by scaffolding core pathway members and by recruiting the scaffold protein Schip1, which promotes Hpo phosphorylation by Tao-1 (Baumgartner et al., 2010; Boggiano et al., 2011; Chung et al., 2016; Genevet et al., 2010; Genevet and Tapon, 2011; Hamaratoglu et al., 2006; McCartney et al., 2000; Poon et al., 2011; Sun et al., 2015; Yu et al., 2010). Ex also directly interacts with WW-domains of Yki at the apical junctions through three PPxY motifs in its C-terminus (Badouel et al., 2009; Oh et al., 2009). This limits the translocation of Yki to the nucleus, as well as bringing it into proximity of the kinase cassette, a process inhibited by Activated cdc42 kinase phosphorylation of Ex (Hu et al., 2016). Together these mechanisms promote robust inhibition of Yki function.

Ex is thought to sit at the interface between the major epithelial polarity axes—apico-basal and planar cell polarity (PCP) since it is regulated by two transmembrane proteins, Fat (Ft) and Crumbs (Crb), which organize tissues by regulating both polarity and growth (Fulford et al., 2018; Genevet and Tapon, 2011). The apico-basal polarity protein Crb promotes Ex apical localization through a direct interaction between the FERM-binding motif of the Crb intracellular domain (ICD) and the N-terminal FERM domain of Ex. Crb is the only transmembrane protein that has been shown to directly bind Ex (Chen et al., 2010; Grzeschik

[1]Department of Developmental Biology, Washington University School of Medicine, St. Louis, USA; [2]Department of Molecular Genetics, University of Toronto, Toronto, Canada; [3]Apoptosis and Proliferation Control Laboratory, The Francis Crick Institute, London, UK.

Correspondence to Helen McNeill: mcneillh@wustl.edu.

et al., 2010; Ling et al., 2010; Robinson et al., 2010). Mutations in *crb* cause mislocalization of Ex from the apical membrane to the cytoplasm, associated with an increase in Yki activity (Chen et al., 2010; Grzeschik et al., 2010; Ling et al., 2010; Robinson et al., 2010). In addition to promoting Ex localization, Crb also regulates Ex levels by promoting its phosphorylation-dependent turnover. Overexpression of Crb stimulates Ex phosphorylation by Casein Kinase 1 (CK1) family kinases. This phosphorylation promotes the interaction of Ex with the F-box E3 ligase Supernumerary Limbs (Slmb) and results in Ex ubiquitination and proteasomal degradation (Fulford et al., 2019; Ribeiro et al., 2014). Ft is a giant atypical cadherin that localizes to the apical junctions where it regulates Hippo signaling and PCP, in part through heterophilic interaction with the atypical cadherin Dachsous (Ds; Blair and McNeill, 2018; Fulford and McNeill, 2020; Irvine and Harvey, 2015). Ft also regulates Ex localization and levels (Bennett and Harvey, 2006; Cho et al., 2006; Silva et al., 2006), however, if Ft regulates Ex directly is not known. The Ft ICD is crucial in implementing its biological function. Several structure-function studies have identified key regions within the ICD that mediate its signaling, including Hippo functional domains and highly conserved regions A to F (Bossuyt et al., 2014; Matakatsu and Blair, 2012; Pan et al., 2013; Zhao et al., 2013; Fig. 1 C and Fig. 4 A).

Ft inhibits growth in part by limiting levels and activity of the atypical myosin Dachs (Mao et al., 2006), which regulates growth by destabilizing and sterically inhibiting Wts, thereby activating Yki function (Cho et al., 2006; Rauskolb et al., 2011; Vrabioiu and Struhl, 2015). Ft suppresses growth in concert with the CK1 kinase Discs overgrown (Dco) and the F-box E3 ubiquitin ligase Fbxl7. Dco phosphorylates the Ft ICD contributing to its activation (Cho et al., 2006; Feng and Irvine, 2009; Pan et al., 2013; Sopko et al., 2009), while Fbxl7 interacts with Ft and limits Dachs accumulation (Bosch et al., 2014; Rodrigues-Campos and Thompson, 2014).

The palmitoyltransferase Approximated (App) and the SH3 containing protein Dlish (also known as Vamana) antagonize Ft activity and promote Dachs activity. Single mutations of *dachs*, *app*, or *dlish* have only mild undergrowth phenotypes alone, but can suppress the overgrowth induced by loss of *ft* (Mao et al., 2006; Matakatsu and Blair, 2008; Misra and Irvine, 2016; Zhang et al., 2016). App, Dlish, and Dachs form a complex at the apical membrane, stabilizing Dachs localization and enhancing its activity (Matakatsu et al., 2017; Matakatsu and Blair, 2008; Misra and Irvine, 2016; Zhang et al., 2016). App can palmitoylate Dlish and regulate Dachs independently of its enzymatic activity (Matakatsu et al., 2017). App also palmitoylates Ft, antagonizing the action of Dco (Matakatsu et al., 2017). The complex relationship between these proteins is thought to precisely tune Hippo pathway activity (Matakatsu et al., 2017).

Ft can regulate Ex localization and levels through Dlish (Wang et al., 2019). Dlish can regulate Hippo signaling independently of Dachs by regulating Ex turnover (Wang et al., 2019). Dlish directly binds to the C-terminus of Ex, promoting the interaction between Ex and Slmb, thereby stimulating Ex degradation via the proteasome. This process is antagonized by Wts phosphorylation at Ex S1116, which stabilizes Ex by protecting it from Slmb-mediated turnover (Zhang et al., 2015). C-terminal regulation of Ex by Slmb appears to be independent of the Crb-mediated regulation of the Ex N-terminus (Fulford et al., 2019). The E3 ubiquitin ligase Plenty of SH3 s has also been implicated in regulating Ex levels by binding to the Ex C-terminus and promoting its degradation (Ma et al., 2018), though this appears to be independent of Dlish (Wang et al., 2019).

Thus, Ex localization, stability, and activity are finely tuned by a complex molecular machinery. However, whether Ft regulation of Ex is direct, the role of Ds in these processes and the relationship between Ft and Crb to control Ex has remained unclear. Here, we report that Ft promotes apical localization of Ex by tethering it to the apicolateral junctional zone, mediated by a direct interaction between the Ex FERM domain and the conserved E region of the Ft ICD. These processes occur independently of Crb. Using CRISPR, we determine that deletion of the conserved E region of Ft leads to wing overgrowth, reduced apical Ex localization, and increased levels of Dachs and Dlish. We show binding between the intracellular domains of Ft and Ds. Remarkably, we find Ft can regulate Ex independently of Ds binding, as loss of *ds* upregulates Dachs/Dlish but does not downregulate Ex. Thus, Fat binding to Ex protects it from degradation, and this protection does not require Fat–Ds binding. This intricate regulation of Ex highlights its importance as an integrator of distinct polarity cues in the control of tissue growth.

Results

Ft and Crb independently regulate Ex levels and localization

Loss of Crb results in the mislocalization of Ex from the apical junction to the cytoplasm in imaginal disc epithelia (Chen et al., 2010; Grzeschik et al., 2010; Ling et al., 2010; Robinson et al., 2010). We confirmed Ex mislocalization in *crb* clones; however, upon close examination we observed that a subset of Ex was still present at the apicolateral junctional zone in the absence of Crb. Residual apical Ex was seen in *crb* null tissue using an Ex-specific antibody or a GFP-tagged knock-in Ex allele (Ex::GFP), and observed in clones of two different *crb* null alleles (Fig. 1, A and B, and Fig. S1, A and B). We confirmed both loss of Crb protein (Fig. S1, C and D) and Ex antibody specificity (Fig. S1 E). These data indicate that there is a portion of Ex that localizes to the apical membrane independently of Crb.

In addition to Crb, Ft regulates Ex localization and levels (Bennett and Harvey, 2006; Cho et al., 2006; Silva et al., 2006; Wang et al., 2019; Fig. 1 C). We confirmed these data and further showed that Crb, Ft, and Ex largely colocalize (Fig. S1, G and H), including within apical puncta where Ft has previously shown to localize (Ma et al., 2003; Brittle et al., 2012; Hale et al., 2015; Fig. S1 I). We also find loss of *ft* does not dramatically affect Crb levels (Fig. S1 J). Interestingly, the remaining apical Ex within *crb* mutant clones colocalizes with Ft (Fig. 1, A and B). We tested the ability of Ft to contribute to Ex apical localization by comparing *crb* null clones and *crb* null clones over expressing full-length, HA-tagged Ft (Ft::HA). Notably, increasing levels of Ft within a *crb* clone significantly rescues apical Ex (Fig. 1, D–F). This

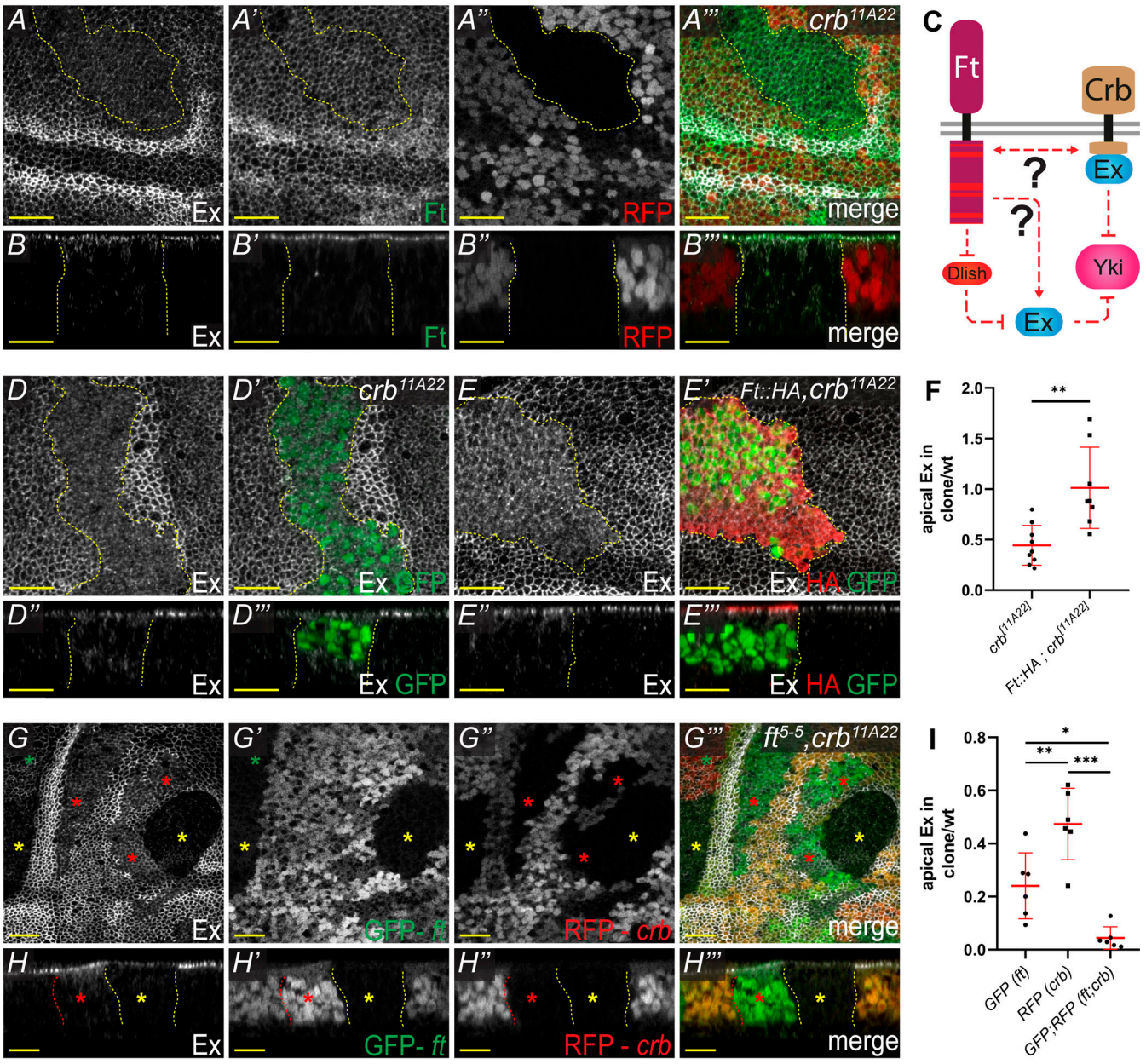

Figure 1. **Ft and Crb regulate Ex independently. (A–B‴)** Loss of Crb does not affect Ft and residual Ex remains at the apical membrane. XY (A–A‴) and transverse (B–B‴) confocal micrographs of third instar wing imaginal discs containing *crb*^{11A22} mutant clones (marked by absence of RFP), with Ex staining (gray in A, A‴, B, and B‴), Ft staining (gray in A′ and B′ and green in A‴ and B‴), and RFP (gray in A″ and B″ and red in A‴ and B‴). **(C)** A model representing the current understanding of Ft and Crb dependent regulation of Ex. Red dashes within the Ft ICD represent the conserved regions A–F. **(D–E‴)** Overexpression of Ft within *crb* mutant tissue rescues apical Ex. XY (D, D′, E, and E′) and transverse (D″, D‴, E″, and E‴) confocal micrographs of third instar wing imaginal discs containing MARCM *crb*^{11A22} clones without UAS-expression (D–D‴) or expressing UAS-Ft::HA (E–E‴). Clones are marked by GFP (green in D′, D‴, E′, and E‴) and are stained with Ex (gray) and Ft (visualized by HA staining, red in E′ and E‴). **(F)** Quantification of the ratio between apical Ex inside versus outside the MARCM clone normalized to the wild-type (wt) tissue. Data points represent an average of a single disc ($n \geq 8$ per genotype) with the mean and SD indicated. **P = 0.0018 using an unpaired *T* test. **(G–H‴)** Loss of Crb and Ft have an additive effect causing dramatic loss of apical Ex. XY (G–G‴) and transverse (H–H‴) confocal micrographs of third instar wing imaginal discs containing *ft*$^{5-5}$ (marked by the absence of GFP—gray in G′ and H′, green in G‴ and H‴, and by green asterisks) and *crb*^{11A22} mutant clones (marked by absence of RFP—gray in G″ and H″, red in G‴ and H‴, and by red asterisks), with Ex staining (gray in G, G‴, H, and H‴). *ft*$^{5-5}$ is a remake of *ft*^{fd} and is a null allele. Double mutant clones are marked by absence of GFP and RFP and by yellow asterisks. **(I)** Quantification of the ratio between apical Ex inside indicated clone verses outside the clone. All quantification was performed on the genotype used to create double clones. Data points represent an average of a single disc ($n = 6$ per genotype) with the mean and SD indicated. *P = 0.0177, **P = 0.0054, and ***P < 0.0001 using one-way ANOVA with a Tukey's post-hoc test. All XY images are orientated as dorsal up and all transverse images are apical up. Clonal boundaries are marked by yellow dotted lines. Scale bars are 10 µm.

increase in apical Ex is not accompanied by alterations in basal Ex (Fig. S1 K) suggesting an overall increase in Ex protein, consistent with previous studies (Bennett and Harvey, 2006; Silva et al., 2006; Wang et al., 2019). This indicates that Ft can promote Ex apical localization and stability independently of Crb.

We next investigated whether Ft regulates Ex localization independently of Crb by examining double-mutant null clones in the wing disc. As *ft* and *crb* are on different chromosomes, FLP (flippase)-FRT (flippase recombinase target)–mediated recombination occurs independently, generating patches of tissue mutant for only *ft* or *crb*, as well as *ft;crb* double-mutant tissue. In the single-mutant tissue, as expected, loss of *crb* or *ft* results in a significant reduction in apical Ex (Fig. 1, G–I). Notably loss of *crb* additionally results in an increase in cytosolic Ex not seen in *ft* mutant clones, consistent with previous studies (Fig. 1 H; Chen et al., 2010; Ling et al., 2010; Robinson et al., 2010). Interestingly, *ft* mutation results in a greater loss of apical Ex than *crb* mutation (Fig. 1 I). In *ft;crb* clones, there is a dramatic and near total loss of Ex when compared to either single mutant (Fig. 1, G–I). Thus, loss-of-function experiments also indicate that Ft and Crb regulate Ex independently.

Ex directly binds to Ft

Both gain- and loss-of-function studies indicate that Ft regulates Ex independently of Crb but do not address how Ft controls Ex localization. To test whether Ft physically associates with Ex, we co-expressed a form of Ft ($Ft^{\Delta ECD}$), which rescues growth defects caused by null mutations of *ft* (Matakatsu and Blair, 2006) with full-length (Ex^{FL}) or the N-terminal FERM domain of Ex (Ex^{FERM}) in $S2R^{+}$ cells (see Fig. 2 C for Ex domains and Ft structure). Both Ex^{FL} and Ex^{FERM} robustly co-immunoprecipitated (co-IP) $Ft^{\Delta ECD}$ (Fig. 2 A), indicating that Ft and Ex can form a biochemical complex.

To determine whether the interaction between Ft and Ex is direct, we performed a pulldown assay between bacterially expressed and purified GST-Ft^{ICD} and in vitro translated N-terminal (Ex^{NT}) and C-terminal Ex (Ex^{CT}) along with GFP as a negative control. Compared to GST alone, GST-Ft^{ICD} significantly binds to Ex^{NT} but not Ex^{CT} (Fig. 2 B). We also tested $Ex^{1\text{-}468}$ and found this smaller fragment of Ex also directly binds Ft^{ICD} (Fig. S2 A). These data reveal Ft binds directly to Ex. These data also indicate the Fat–Ex interaction occurs via the N-terminal Ex FERM domain.

Next, we investigated whether the Ft–Ex interaction occurs in vivo by performing an in situ proximity ligation assay (PLA), an immuno-PCR-based technique producing a positive fluorescent signal when two antibody epitopes are no further than ∼40 nm apart and presumably interacting directly (Alam, 2018). In addition, PLA provides data on the localization of protein interactions. To perform this technique, we used the FERM-domain containing $Ex^{1\text{-}468}$ truncation, driven by the *ubiquitin 63E* promoter (ubi-$Ex^{1\text{-}468}$::GFP; Fulford et al., 2019), which colocalizes with Ft (Fig. S2 B) and a C-terminal FLAG-tagged Ft knock-in allele we generated for this study. Consistent with our biochemical data, we observed PLA signal colocalizing with Ex signal at the apicolateral junctional zone in XZ (Fig. 2 D) and XY (Fig. S2 C) sections of imaginal wing discs, supporting a direct interaction in vivo between Ft and Ex.

Dlish has recently been shown to directly bind the C-terminus of Ex and regulate its turnover downstream of Ft (Wang et al., 2019). Dlish and Ft have been shown to interact via co-IP from cultured cells (Misra and Irvine, 2016; Zhang et al., 2016) but it is unclear if this interaction is direct. We therefore tested whether Dlish could also bind FtICD through an in vitro binding assay similarly to Ex but could see no evidence of direct binding (Fig. S2 D). Taken together, these data support the hypothesis that the Ex FERM domain binds directly to Ft in vivo at the apical membrane and suggest a model where Ex biochemically links Ft and Dlish.

Ft contains two Ex interaction domains

Our data indicate that the Ft ICD binds directly to the Ex FERM (Fig. 2 B and Fig. S2 A). To determine which region of Ft interacts with the FERM domain, we performed co-IPs using truncated and/or internally deleted $Ft^{\Delta ECD}$ constructs in HEK293 cells (see Fig. 3 E and Fig. S3 C). Significantly, $Ft^{c\Delta 244}$ (removing 244 residues from the C-terminus of $Ft^{\Delta ECD}$) can effectively co-IP Ex^{FERM}, whereas removing 255 residues from the C-terminus of $Ft^{\Delta ECD}$ ($Ft^{c\Delta 255}$) completely abolished the interaction with Ex^{FERM} (Fig. 3 A). These data indicate the amino acids between residues 255–244 from the Ft C-terminus are needed to interact with Ex^{FERM}, defining Expanded Binding Region 1 (EBR1). Interestingly, this region is within the Hippo activating domain of the Ft ICD as defined in several structure-function analyses of Ft (Bossuyt et al., 2014; Matakatsu and Blair, 2012; Pan et al., 2013; Zhao et al., 2013; Fig. 3 E and Fig. 4 A).

Further deletion and co-IP analyses revealed the existence of a second Ex binding site in the C-terminus of Ft (Fig. S3 A). This binding site includes the E and F domains (defined in Pan et al., 2013), conserved across multiple species including human FAT4. To confirm this interaction, we generated a construct containing the last 124 residues of Ft tagged with a myristoylation sequence targeting it to cell membranes ($Ft^{myr\text{-}c124}$). $Ft^{myr\text{-}c124}$ can interact with Ex^{FERM} (Fig. 3 B), indicating that the C-terminal 124 residues of Ft can bind Ex. To narrow down the C-terminal binding domain further, we created an internal deletion within $Ft^{myr\text{-}c124}$, which removes a Ft ICD fragment containing the conserved E region ($Ft^{myr\text{-}c124;\Delta EBR2}$). This deletion abolished the interaction between Ft and Ex (Fig. 3 B) indicating an Ex-binding region lies between the C-terminal residues 64–25, which we named EBR2 (Fig. 3 E and Fig. 4 A). Interestingly, neither EBR1 nor EBR2 contain known FERM binding motifs (Gunn-Moore et al., 2006; Ling et al., 2010).

We confirmed a direct interaction between Ft conserved E region and Ex by generating a biotin-tagged peptide—called $EBR2^{WT}$—and performed a streptavidin-pulldown with recombinant Ex^{NT} (Fig. 3 C). In contrast, a biotin-tagged EBR^{MUT} peptide, with six residues mutated to alanine, was unable to interact with Ex^{NT}, highlighting the importance of the conserved E region in the binding to Ex (Fig. 3 C).

To explore whether additional conserved regions affect the Ft–Ex interaction, we generated $Ft^{\Delta ECD}$ constructs from EBR1 through to the conserved D region ($Ft^{c\Delta 492\text{-}256;c\Delta 153}$), removing the C region ($Ft^{c\Delta 492\text{-}256;\Delta C;c\Delta 153}$), D region ($Ft^{c\Delta 492\text{-}256;\Delta D\text{-}CT}$), or

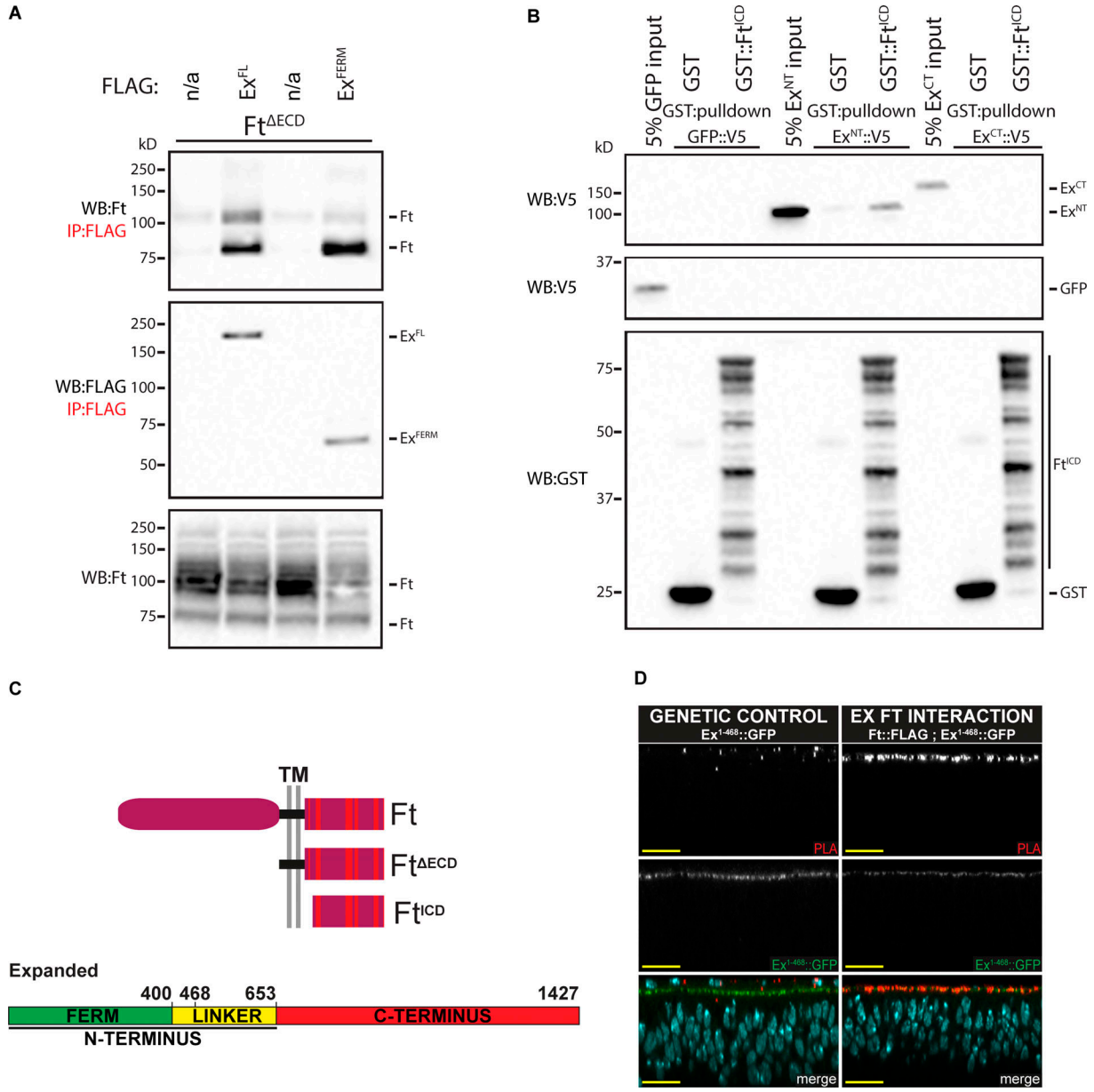

Figure 2. **Ft and Ex directly bind in vitro and interact at apicolateral regions in vivo. (A)** $Ft^{\Delta ECD}$ interacts with Ex^{FL} and Ex^{FERM}. S2R+ cell expression and IP of FLAG-tagged Ex^{FL} or Ex^{FERM} in the presence of $Ft^{\Delta ECD}$, compared to FLAG-bead controls. Ft presents as multiple bands due to proteolytic processing (Feng and Irvine, 2009; Sopko et al., 2009). n/a indicates no Flag-tagged protein added. **(B)** Ft^{ICD} directly binds Ex^{NT}. In vitro transcribed and translated GFP as a control, Ex^{NT} and Ex^{CT} were incubated with bacterially expressed and purified GST alone or GST::Ft^{ICD} and subjected to GST-purification. The expression and presence of proteins was analyzed by immunoblotting with the indicated antibodies. **(C)** Schematic representation of Ft, $Ft^{\Delta ECD}$ and Ft^{ICD} and Ex protein. Red dashes within the Ft ICD represent the conserved regions A–F. **(D)** Ft and Ex interact at apical membrane in vivo. Transverse confocal micrographs of third instar imaginal discs expressing *ubi-Ex*$^{1\text{-}468}$*::GFP* subjected to anti-FLAG and anti-GFP PLA. Genetic control expresses only *ubi-Ex*$^{1\text{-}468}$*::GFP* with wild-type Ft, and the Ex::Ft interaction condition expresses *ft::FLAG* at the endogenous locus and *ubi-Ex*$^{1\text{-}468}$*::GFP*. $Ex^{1\text{-}468}$::GFP is observed by direct fluorescence of GFP (gray or green in merge), PLA signal (gray or red in merge) marks interaction loci, and Hoechst (cyan in merge) marks nuclei. Sections are orientated apical up. Scale bars are 10 µm. WB, Western blot. Source data are available for this figure: SourceData F2.

both ($Ft^{c\Delta 492\text{-}256;\Delta C;\Delta D\text{-}CT}$). Interestingly, we found that loss of either of these conserved regions reduced Ft–Ex interaction, and removal of both completely abolished it, although these constructs contain EBR1 (Fig. S3 B). These data show that the conserved C and D regions contribute to the Ft–Ex interaction. Deleting the entire region from EBR1 to EBR2 ($Ft^{\Delta EBR1\text{-}EBR2}$) abrogates Ex binding (Fig. 3 D).

Ex binding regions of the Ft ICD are required in vivo for regulation of tissue growth

Having mapped the regions of the Ft ICD that interact with Ex, we next investigated their biological significance in vivo. We used CRISPR to delete EBR1 (Ft^{EBR1}) and both EBR1 and EBR2 ($Ft^{EBR1/2}$), from the endogenous *ft* locus, and added a 3xFLAG tag to the C-terminus. In addition, we used CRISPR to remove the

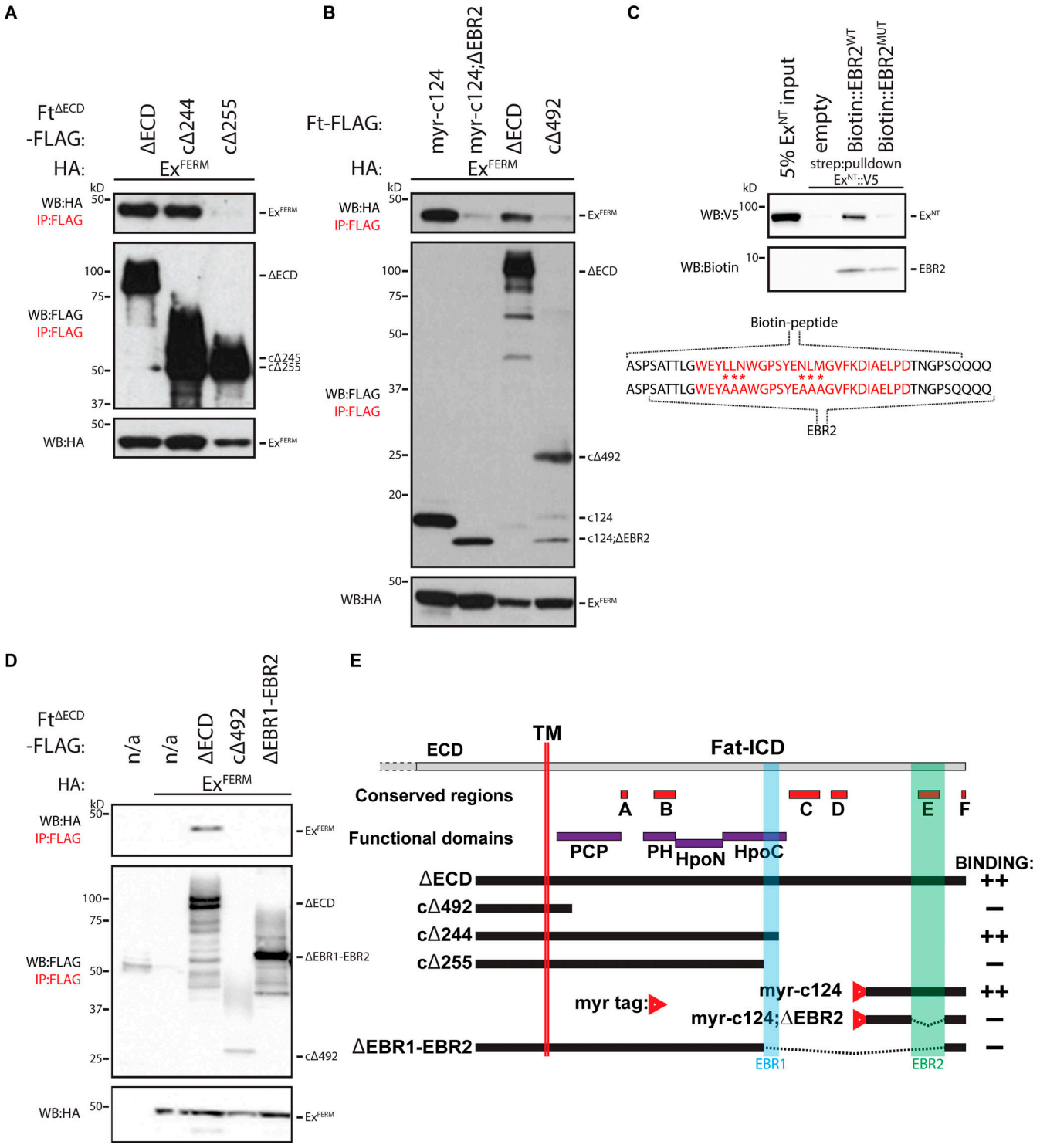

Figure 3. **Identification of EBRs within the Ft ICD. (A)** Identification of EBR1 in the Ft ICD. HEK293 cell expression and IP of indicated FLAG-tagged $Ft^{\Delta ECD}$ constructs in the presence of Ex^{FERM}. **(B)** Identification of EBR2 in the Ft ICD. HEK293 cell expression and IP of indicated FLAG-tagged $Ft^{\Delta ECD}$ or FLAG- and myristoyl-tagged constructs in the presence of Ex^{FERM}. **(C)** EBR2 directly binds Ex^{NT}. In vitro transcribed and translated Ex^{NT} was incubated alone or with biotin-tagged $EBR2^{WT}$ or $EBR2^{MUT}$ peptide (sequences indicated—mutant peptide containing six alanine substitutions) and subjected to streptavidin-purification. EBR2 sequence defined by co-IP and the conserved E region (highlighted in red) are also indicated. **(D)** Identification of the Ex interacting region of the Ft ICD. HEK293 cell expression and IP of indicated FLAG-tagged $Ft^{\Delta ECD}$ constructs in the presence of Ex^{FERM} compared to FLAG-bead controls. The expression and presence of proteins was analyzed by immunoblotting with the indicated antibodies. Ft presents as multiple bands due to proteolytic processing (Feng and Irvine, 2009; Sopko et al., 2009). n/a indicates no Flag-tagged protein added. **(E)** Graphical scheme highlighting the Ft constructs used in the figure. In addition, the transmembrane domain (TM), EBR1, EBR2, and established conserved and function domains of the Ft ICD are depicted. In binding column: "++" denotes constructs that interact strongly to Ex^{FERM} and "–" denotes no interaction with Ex^{FERM}. WB, Western blot. Source data are available for this figure: SourceData F3.

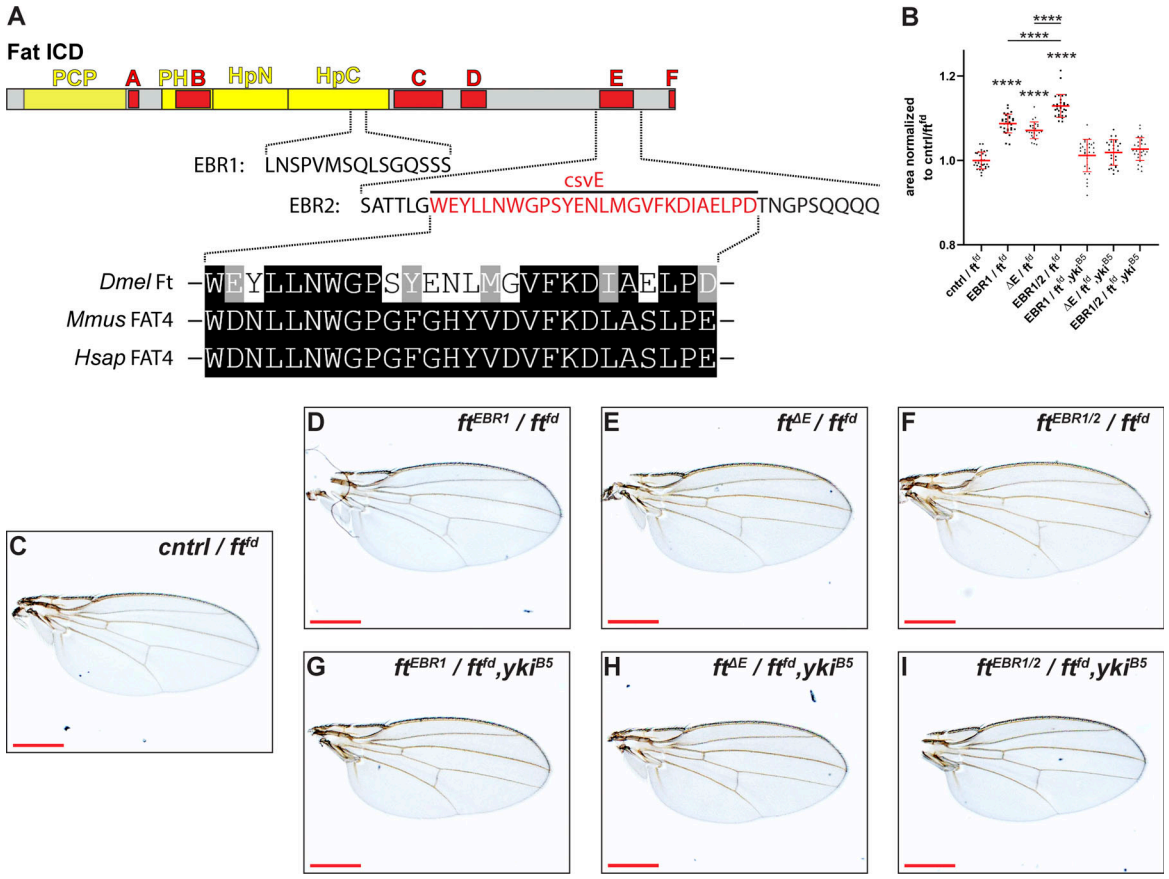

Figure 4. **EBRs are required in vivo for regulation of tissue growth. (A)** Schematic representation of the Ft ICD highlighting functional and conserved domains. EBR1, EBR2, and conserved E location and amino acid sequence are depicted, in addition to the conservation of the conserved E region (in red) between flies, mice, and humans. EBR1 and EBR1/2 flies have the indicated sequences removed and have a C-terminal 3× FLAG. Conserved E has the indicated sequence (highlighted in red) replaced with a 3× FLAG. **(B)** Quantification of adult wing size with haploinsufficiency for *ft* or *ft, yki*. Data are normalized against the mean of the *cntrl/ft^{fd}* (*ft::FLAG/ft^{fd}*). All EBR flies are overgrown, with ft$^{EBR1/2}$ causing additive overgrowth. Haploinsufficiency of *ft, yki* rescues overgrowth (****significance for ft^{EBR1}, ft$^{\Delta E}$ and ft$^{EBR1/2}$ compared to the respective genotypes haploinsufficient for *ft* alone). Data points indicate an individual wing with mean and SD represented ($n \geq 27$ per genotype). ****P < 0.0001 using one-way ANOVA with a Tukey's post-hoc test compared to *cntrl/ft^{fd}* or between indicated genotypes. **(C–I)** EBR deletion causes overgrowth and is rescued by haploinsufficiency of *yki*. Compared to control wings—ft::FLAG (C), loss of *ft^{EBR1}* (D), *ft$^{\Delta E}$* (E), and *ft$^{EBR1/2}$* (F) cause overgrowth when over the null *ft^{fd}* allele. Additional loss of one copy of *yki* rescues overgrowth of all indicated genotypes *ft^{EBR1}* (G), *ft$^{\Delta E}$* (H), and *ft$^{EBR1/2}$* (I). Scale bars are 500 µm.

conserved E region (largely overlapping EBR2), and replaced it with a 3xFLAG tag (Ft$^{\Delta E}$; Fig. 4 A). Immunoblot and clonal analysis indicated deletion of these regions in Ft^{EBR1}, Ft$^{\Delta E}$, and Ft$^{EBR1/2}$ did not affect levels of Ft protein, nor perturb Ft localization (Fig. S4, A–D). To account for CRISPR-induced second site hits, we performed trans-heterozygous analysis of two independent lines for each mutation, which produced viable and fertile animals for all genotypes (Fig. S4, E–I) despite significant pupal lethality in Ft$^{\Delta E}$ and Ft$^{EBR1/2}$ (Fig. S4 J). Due to the pupal lethality seen in Ft$^{\Delta E}$ and Ft$^{EBR1/2}$, we analyzed wing growth phenotypes as trans-heterozygous to the *ft^{fd}* null allele. Interestingly, in this sensitized background, all three genotypes produced overgrown wings compared to the ft::FLAG control, with Ft$^{EBR1/2}$ producing overgrowth in excess of either Ft^{ERB1} or Ft$^{\Delta E}$ (Fig. 4, B–F).

Further analysis of the EBR trans-heterozygous flies (independent lines of the same mutation) confirmed Ft^{EBR1} causes wing overgrowth, consistent with EBR1 residing in the HpoC functional domain that affects Hippo signaling (Fig. S4, E and F, K). However, Ft$^{\Delta E}$ flies were not overgrown (Fig. S4, G and K), and Ft$^{EBR1/2}$ wings were mostly undergrown (class 1; Fig. S4, H and K), with a distinct subpopulation of Ft$^{EBR1/2}$ flies (class 2) that were significantly larger than the controls (Fig. S4, I and K). The reason for this phenotypic separation remains unclear but could be due to developmental defects causing the significant pupal lethality observed (Fig. S4 J). Nevertheless, the population of Ft$^{EBR1/2}$ flies that were overgrown (class 2) all had rounded wings with cross-vein defects (Fig. S4 I), which was also observed in Ft$^{\Delta E}$ (Fig. S4 G), indicating the E region affects wing shape. We calculated the ratio of length to width to measure the wing roundness, a typical phenotype of Ft/Ds pathway mutants (Mao et al., 2006; Matakatsu and Blair, 2006). Both Ft^{EBR1} and Ft$^{\Delta E}$ had significantly rounder wings than controls (Fig. S4 L). As with wing size, Ft$^{EBR1/2}$ separated into distinct populations, with the class 2 subpopulation generating wings that were significantly rounder than the control (Fig. S4 L).

To assess whether the overgrowth was the result of excessive Yki activity, we analyzed adult wing phenotypes in a *ft, yki* haplo-insufficient background. Importantly, overgrowth of EBR mutant flies was suppressed when one copy of Yki was removed, consistent with the hypothesis that overgrowth due to loss of Ex binding to Ft is Hippo pathway dependent (Fig. 4, B–I).

Conserved E region/EBR2 is required to regulate Ex, Dachs, and Dlish in vivo

To mechanistically understand the effects of loss of Ex binding regions on the Hippo pathway, we generated mitotic clones of our new alleles in wing discs and stained for Ex, as well as for Dlish and Dachs, critical mediators of Ft–Hippo signaling (Mao et al., 2006; Misra and Irvine, 2016; Zhang et al., 2016). Ft restricts Dlish and Dachs apical localization, and Dlish stimulates Ex degradation (Wang et al., 2019). Loss of Ft leads to reduction of Ex (Fig. S1 F) and increased expression of Dachs and Dlish as previously reported (Bennett and Harvey, 2006; Mao et al., 2006; Misra and Irvine, 2016; Silva et al., 2006; Zhang et al., 2016). Clones of cells homozygous for ft^{EBR1} caused no change in levels or distribution of Ex, Dachs, or Dlish (Fig. 5, A, D, and G), indicating this region is not critical for regulation of these proteins. Importantly, clones of $ft^{\Delta E}$ or $ft^{EBR1/2}$ showed a reduction in apical Ex (Fig. 5, B and C), and a dramatic increase in both Dlish and Dachs (Fig. 5, E, F, H, and I). Together, these data indicate that conserved region E is essential for restricting Dlish and Dachs and stabilizing Ex in vivo. Interestingly, $ft^{EBR1/2}$ clones appear to cause a greater loss of apical Ex than $ft^{\Delta E}$, which may indicate a contribution of EBR1 (Fig. 4 A).

As Crb and Dlish both regulate Ex, we wondered whether loss of Crb alters Dachs/Dlish, and therefore regulate Ex through these proteins. Neither Dachs nor Dlish was altered in *crb* clones (Fig. S5, A and B), indicating that Ft and Crb independently regulate Ex. As Dlish binds to the Ex C-terminus, these data are also consistent with previous studies showing the Slmb-mediated regulation of the Ex C-terminus is independent of Crb (Fulford et al., 2019).

Loss of Fbxl7 increases apical Dachs (Bosch et al., 2014; Rodrigues-Campos and Thompson, 2014). As increased apical Dachs is associated with a concurrent increase in apical Dlish, we investigated whether loss of Fbxl7 could also regulate Ex. Knockdown of Fbxl7 did not alter levels of endogenous Ex observed through staining, or levels of the ubi-$Ex^{1\text{-}468}$::GFP construct that does not respond to changes in Yki transcription (Fig. S5, C and D). These data suggest Fbxl7 does not regulate Ex.

Dachs and Dlish levels increase in Ds mutants, but Ex levels are not reduced

Ds is the only known ligand of Ft, and spatial gradients of Ds expression are thought to regulate Ft activity (Strutt and Strutt, 2021). Null mutations of *ft* or *ds* result in increased levels of apical Dachs and Dlish and Hippo pathway–dependent overgrowth (Brittle et al., 2012; Misra and Irvine, 2016; Zhang et al., 2016). We confirmed Ds repression of Dachs and Dlish, generating clones of ds^{38k}, a protein null (Fig. S5 E). *ds* clones display clear increases in both Dachs and Dlish (Fig. S5, F and G). We also stained *ds* clones for Crb and observed no change (Fig. S5 H).

Given the current model where increased levels of Dlish–Ex complex stimulates Ex degradation (Wang et al., 2019), loss of Ds should lead to reduced Ex. We therefore investigated whether Ds regulates Ex. Remarkably, *ds* loss in wing discs did not decrease Ex levels and often resulted in a subtle increase in Ex, particularly in the imaginal disc hinge region, where Ds expression is highest (Fig. S5, J and K). This is in stark contrast to *ft* mutant clones, which dramatically decrease Ex (Fig. S1 F). Loss of *ds* has a limited effect on Ft staining in the wing pouch, with subtly diffuse but still apical Ft (Strutt and Strutt, 2021; Mao et al., 2009; Fig. S5 I). These surprising data indicate that, despite Ds regulating Dachs and Dlish, there is no reciprocal reduction in Ex, and further indicate that levels of Dachs/Dlish can be uncoupled from levels of Ex.

Our finding that Ft and Ds both regulate Dachs and Dlish levels, yet loss of Ds does not cause a reduction in Ex, prompted us to investigate whether Ds and Ex could bind. However, we found no evidence of a direct interaction between Ds and Ex^{NT} or Ex^{CT}, consistent with Ft regulation of Ex being independent of Ds (Fig. S5 J). As Ds and Dlish interact through co-IP (Misra and Irvine, 2016; Zhang et al., 2016), we tested whether they could directly bind, but found no interaction (Fig. S5 K) suggesting these proteins likely need an intermediary to interact.

Ds and Ft directly bind to each other via cytoplasmic domain interactions

Although representations of Ft and Ds emphasize asymmetric distribution of these molecules, co-staining reveals that there is substantial overlap in Ft and Ds staining at cell membranes (Ma et al., 2003). In addition, Ds puncta visualized by immunofluorescence are stabilized by the presence of Ft (Hale et al., 2015), and genetic data suggest that Ft and Ds may interact in cis (within cells) as well as in trans (Sharma and McNeill, 2013).

We therefore tested whether Ft and Ds could interact independently of their previously documented extracellular domain interactions by performing co-IP of $Ft^{\Delta ECD}$ with Ds^{ICD} in S2R + cells. $Ft^{\Delta ECD}$ removes most of the extracellular domain, including all cadherin repeats, EGF-like domains and Laminin-G domains, and retains the transmembrane domain, and the full ICD (Matakatsu and Blair, 2006). Ds^{ICD} removes the entire extracellular and transmembrane domains, and only retains the intracellular domain. Remarkably, Ds ICD can co-immunoprecipitate with $Ft^{\Delta ECD}$ (Fig. 5 L), indicating that Ft and Ds can form a complex mediated by their cytoplasmic domains.

The co-IP of Ft and Ds mediated by their intracellular domains could be direct, or via intermediary proteins. We tested whether this interaction was direct through a binding assay between GST-Ft^{ICD} and in vitro translated Ds^{ICD} and observed binding between the ICDs of these proteins (Fig. 5 M). These data indicate cis interactions between Ft and Ds within the cytoplasm can be mediated via their ICDs. Thus, Ft and Ds can interact both across cell borders via their extracellular cadherin repeats, and within cells via their intracellular domains. These intracellular interactions imply that complexes that are independently formed on Ft and Ds can be brought together, and this cross-regulation has the potential for regulating Hippo or PCP activity.

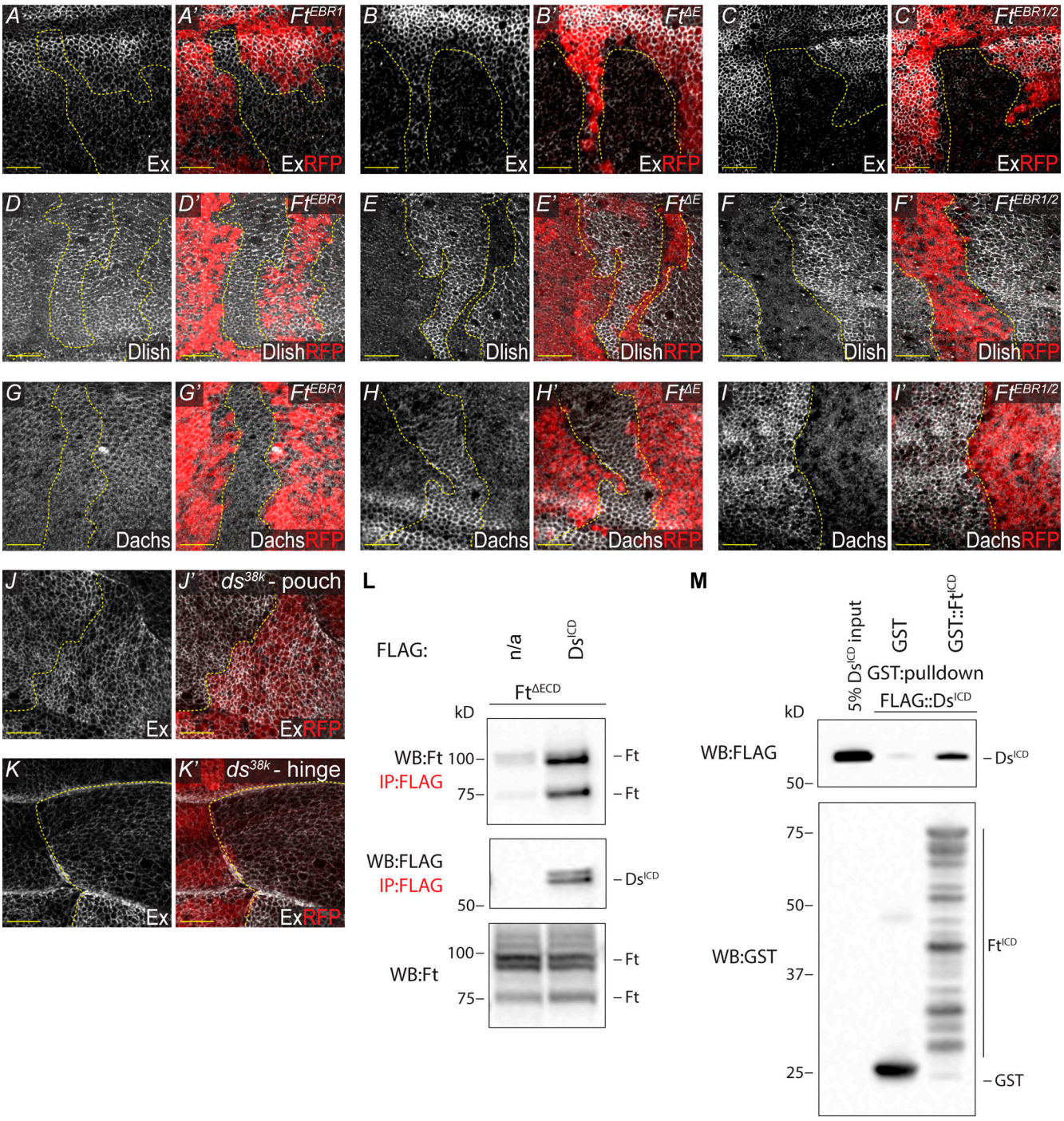

Figure 5. **EBR clonal analysis and Ft–Ds interaction. (A–C′)** $ft^{\Delta E}$ and $ft^{EBR1/2}$ cause a reduction of apical Ex, unlike ft^{EBR1}. XY confocal micrographs third instar wing imaginal discs containing ft^{EBR1} (A and A′), $ft^{\Delta E}$ (B and B′), and $ft^{EBR1/2}$ (C and C′) mutant clones (marked by absence of RFP shown in red) with Ex staining (shown in gray). **(D–I′)** $ft^{\Delta E}$ and $ft^{EBR1/2}$ cause an increase of apical Dlish and Dachs, unlike ft^{EBR1}. XY confocal micrographs third instar wing imaginal discs containing ft^{EBR1} (D, D′, G, and G′), $ft^{\Delta E}$ (E, E′, H, and H′) and $ft^{EBR1/2}$ (F, F′, I, and I′) mutant clones (marked by absence of RFP shown in red) with Dlish (D–F′) or Dachs (G–I′) staining (shown in gray). **(J–K′)** Loss of *ds* subtly increases Ex. XY confocal micrographs of the same third instar wing imaginal disc showing the pouch (J and J′) and the hinge (K and K′) containing ds^{38K} mutant clones (marked by absence of RFP shown in red) with Ex staining (shown in gray). All XY images are orientated as dorsal up. Clonal boundaries are marked by yellow dotted lines. Scale bars are 10 µm. **(L)** $Ft^{\Delta ECD}$ interacts with Ds^{ICD}. $S2R^{+}$ cell expression and IP of FLAG-tagged Ds^{ICD} in the presence of $Ft^{\Delta ECD}$, compared to FLAG-bead controls. Ft presents as multiple bands due to proteolytic processing (Feng and Irvine, 2009; Sopko et al., 2009). **(M)** Ft^{ICD} directly binds Ds^{ICD}. In vitro transcribed and translated Ds^{ICD} was incubated with bacterially expressed and purified GST alone or GST::Ft^{ICD} and subjected to GST-purification. The expression and presence of proteins was analyzed by immunoblotting with the indicated antibodies. WB, Western blot. Source data are available for this figure: SourceData F5.

Discussion

Ex is a critical nexus of Hippo signaling and is highly regulated, with its levels and localization being controlled by two transmembrane proteins, Crb and Ft (Bennett and Harvey, 2006; Ling et al., 2010; Fulford et al., 2019; Ribeiro et al., 2014; Silva et al., 2006; Wang et al., 2019). Cell–cell interactions are a key aspect of Hippo pathway upstream regulation that is thought to underpin their role in maintaining tissue homeostasis (Fulford et al., 2018; Misra and Irvine, 2018; Zheng and Pan, 2019). Previously, Crb was the only transmembrane protein known to directly bind and regulate Ex function (Ling et al., 2010), and has been established as an apical hub of Hippo signaling (Genevet and Tapon, 2011; Su et al., 2017; Sun et al., 2015). Here we show that both Crb and Ft directly bind to Ex and regulate Ex independently. Loss of Ft in the absence of Crb further reduces apical Ex localization and overexpression of Ft in *crb* mutant tissue is sufficient to rescue apical Ex levels, consistent with increased Ex protein (Fig. 1, D–I, and Fig. S1 K). Meanwhile, loss of *crb* does not affect Dachs or Dlish, which regulate Ex downstream of Ft (Fig. S5, A and B). These data demonstrate the ability of Ft to recruit and stabilize Ex apically, independently of Crb.

We show Ft interacts with the Ex FERM domain at the apical membrane (Fig. 2, B and D, and Fig. S2, A and C), largely at junctions, potentially occurring through direct binding of Ex with the Ft conserved E region (Fig. 3 C). Removal of the EBRs leads to wing overgrowth, although the extent of this overgrowth depends on the genetic background (Fig. 4 and Fig. S4). Haploinsufficiency for *yki* rescues EBR mutant wing overgrowth (Fig. 4, B–I) and loss of conserved region E alters the localization of the Hippo pathway regulators Ex, Dachs, and Dlish (Fig. 5, A–I). Combined, these data indicate that this conserved region regulates Hippo signaling, and that Ft interaction with Ex provides a Crb-independent hub for Hippo signaling at the apicolateral junctional zone.

While several Hippo pathway proteins have been identified as interacting with Ft (App, Dco, Dlish, Ds, FbxL7, Fj, and Lft), or are regulated by Ft, so far none have been identified as a direct intracellular binding partner (Bosch et al., 2014; Brittle et al., 2010; Feng and Irvine, 2009; Ishikawa et al., 2008; Mao et al., 2009; Matakatsu et al., 2017; Sopko et al., 2009; Matakatsu and Blair, 2004; Misra and Irvine, 2016; Simon et al., 2010; Zhang et al., 2016).

We show here that Ex binds directly to Ft. Ex also binds directly to Dlish, which promotes Slmb-dependent proteasomal degradation of Ex (Wang et al., 2019). Ex-Dlish binding occurs through the Ex C-terminus, whereas Ft binds to the N-terminal Ex FERM domain (Fig. 2 B). The region of the Ft ICD which interacts with Dlish (Zhang et al., 2016) overlaps with the conserved E region that binds Ex. Therefore, Dlish may interact with Ft via Ex. In the simplest model, a Ft–Ex–Dlish complex may conformationally inhibit Dlish, sequestering it away from Ex and preventing Ex degradation (Fig. 6). Alternatively, the Ft–Ex–Dlish complex could inhibit the ability of App to palmitoylate Ft and/or Dlish (Matakatsu et al., 2017; Zhang et al., 2016). In this case, the Ex–Ft interaction would promote Ft signaling and limit the apical localization of Dlish and Dachs, therefore inhibiting Dlish-dependent Ex degradation. Moreover, App antagonizes activating phosphorylation of Ft by the CK1 kinase Dco (Matakatsu et al., 2017). We note residual apical Ex when both *crb* and *ft* are lost (Fig. 1, G and H), suggesting there are additional mechanisms to regulate apical Ex, such as Ex interaction with apical Spectrins (Fletcher et al., 2015).

Unexpectedly, although loss of Ds results in increased Dachs/Dlish, Ex levels do not decrease (Fig. 5, J and K, and Fig. S5, F and G). We hypothesize that increased Dachs/Dlish levels are unable to stimulate Ex degradation in *ds* mutant cells because unbound Ft can still bind Ex, protecting it from Dlish-dependent degradation (Fig. 6). This is consistent with the ability of Ft to suppress growth independently of Ds (Matakatsu and Blair, 2006). Together our data show Ft both directly contributes to apical localization of Ex and promotes Ex stability, ensuring consistent levels of Ex protein, and Hippo pathway homeostasis.

We also discovered that in addition to their known extracellular trans interaction (Brittle et al., 2010; Matakatsu and Blair, 2004; Simon et al., 2010), the Ft and Ds ICDs interact directly via their cytoplasmic domains (Fig. 5, L and M). Previous studies have shown that although loss of Ds promotes growth, the Ds ICD itself can promote growth. This may occur through interaction with Dachs and Dlish to promote their activity (Bosveld et al., 2012; Misra and Irvine, 2016; Zhang et al., 2016)

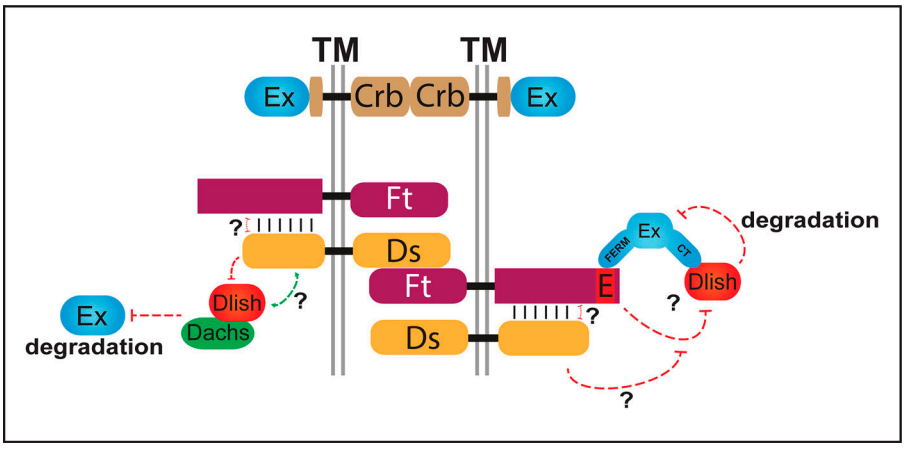

Figure 6. **A model of Ft-mediated regulation of Ex.** Graphical illustration of findings (not to scale). In wild-type conditions, Ft regulates Ex independently of Crb and there is a homeostasis of Ex levels. Ft promotes apical localization of Ex. Degradation of Ex is stimulated by Dlish, which is balanced by Ft-mediated inhibition of Dlish. Loss of Ds increases the amount of apical Dlish available to interact with and degrade Ex, however this is counteracted by Ft actively inhibiting this process. Upon loss of Ft, or the conserved E region responsible for Ft–Ex interaction, Dlish is derepressed, increasing Ex degradation. Ft and Ds cis interaction may act to antagonize Ft-mediated inhibition of Dlish, which may also promote mutual antagonism between Ft and Ds to support PCP. TM, transmembrane domain.

and through the phosphorylation and inhibition of Wts by the Minibrain kinase (Degoutin et al., 2013).

The subtle increase in Ex within *ds* clones (Fig. 5, J and K) despite the strong increase in Dachs and Dlish suggests another potential mechanism by which the Ds ICD can promote growth—by antagonizing Ft to promote Ex degradation. This could be influenced by the interaction of the Ft–Ds ICDs and suggests binding, in trans and cis, may modulate the interaction of Ft–Ex and Hippo signaling more broadly (Fig. 6).

Ft–Ex binding is dependent on regions that are highly conserved in Ft orthologues, including in mammals (Fig. 4 A). Interestingly, in mammals, Fat4 and Crb3 both regulate a functional orthologue of Ex, Amot. In mammalian cells, Amot binds to the Crb3 complex to regulate YAP/TAZ activity and, in the heart, Fat4 binds to Amotl1 to mediate YAP1 nuclear exclusion (Ragni et al., 2017; Varelas et al., 2010). It will be interesting to see whether the conserved regions of Fat4 contribute to its interaction with Amotl1 or other FERM domain orthologues of Ex to regulate YAP signaling.

Materials and methods

Drosophila genetics and genotypes

Ex::GFP and $ft^{5\text{-}5}$ were generated by CRISPR/Cas9-mediated gene editing. *Ex::GFP* contains a C-terminal GFP tag. The *ex* genomic locus was cut near the stop codon by Cas9 guided by a gRNA (sequence: 5′-ATTAGCTTGTCGAGTCTAGC-3′) and repaired from a co-injected plasmid template containing homologous sequence from the *ex* locus (2.4 kb upstream and 2.0 kb downstream of the stop codon), in which the eGFP coding sequence had been inserted immediately before the ex stop codon. $ft^{5\text{-}5}$ is a remake of the ft^{fd} allele. The entire Ft locus was sequenced in wild-type *yw* and mutant ft^{fd} flies, which identified a single nucleotide mutation in Tyr982 (TAT > TAA) generating a premature stop codon in the first exon. This mutation was regenerated using Cas9 guided by gRNA (sequence: 5′-GGGATG CGGGCGTGAATAGT-3′) and repaired from a co-injected plasmid template containing homologous sequence (1.3 kb upstream and 1.3 kb downstream of the ft^{fd} mutation site) incorporating site directed mutagenesis to generate the T > A mutation. Progeny were genotyped and validated by sequencing.

ft::FLAG, ft^{EBR1}*::FLAG*, and $ft^{EBR1/2}$*::FLAG*, all with C-terminal 3× FLAG tags and $ft^{\Delta E}$*::FLAG* with the conserved E region replaced by a 3× FLAG tag were generated by CRISPR/Cas9-mediated gene editing performed by GenetiVision. Sequences removed or replaced are indicated in Fig. 4 A. Two independently generated lines for each genotype were analyzed: *ft::FLAG (2)* and *(5)*, ft^{EBR1}*::FLAG (1-1)* and *(3-2)*, $ft^{\Delta E}$*::FLAG (1–2)* and *(5-2)* and $ft^{EBR1/2}$*::FLAG (1–5)* and *(4-3)*. Genotypes were validated by sequencing.

$dlish^{BI60I}$ was obtained from Seth Blair (University of Wisconsin-Madison, Madison, WI, USA). Transgenic RNAi *fbxl7: HMJ22830* was obtained from Bloomington (BL60461).

All crosses were raised at 25°C. Mitotic clones were induced using *hsFLP* by incubating the larvae at 37°C for 1 h, 48 h after egg laying or for 1 h at both 48 and 72 h after egg laying.

Specific genotypes described below:

Fig. 1, A and B′′′; Fig. S1, C and D′; Fig. S5, A and B′: *hsFLP;; FRT82B, ubi-mRFP.nls/FRT82B,* crb^{11A22}

Fig. 1, D and D′: tub-Gal4, hsFLP, UAS-nls.GFP::myc;; FRT82B, tub-Gal80/FRT82B, crb11A22

Fig. 1, E and E′: tub-Gal4, hsFLP, UAS-nls.GFP::myc; UAS-Ft::HA/+; FRT82B, tub-Gal80/FRT82B, crb11A22

Fig. 1, G and H′′′: hsFLP; ubi-GFP, FRT40A/ft5-5, FRT40A; FRT82B, ubi-mRFP.nls/FRT82B, crb11A22

Fig. S1, A and A′: hsFLP; ex::GFP/+; FRT82B, ubi-mRFP.nls/FRT82B, crb11A22

Fig. S1, B and B′: hsFLP; ex::GFP/+; FRT82B, ubi-mRFP.nls/FRT82B, crb82-04

Fig. S1, E and E′: hsFLP; ubi-mRFP.nls, FRT40A/exe1, FRT40A

Fig. S1, F and F′; J and J′: hsFLP; ubi-mRFP.nls, FRT40A/ft5-5, FRT40A

Fig. S1, G and G′′′: ; ex::GFP/ex::GFP

Fig. S1. H and I′′′: w1118

Fig. 2 D: genetic control

Fig. S2, B and B′′′: ;; ubi-Ex1-468::GFP/ubi-Ex1-468::GFP

Fig. 2 D and Fig. S2 C—Ex::Ft Interaction: ; ft::FLAG (2)/ft::FLAG (2); ubi-Ex1-468::GFP/ubi-Ex1-468::GFP

Fig. 4 C: ; ft::FLAG (2)/ftfd

Fig. 4 D: ; ftEBR1::FLAG (1-1)/ftf

Fig. 4 E: ; ftΔE::FLAG (5-2)/ftfd

Fig. 4 F: ; ftEBR1/2::FLAG (4-3)/ftfd

Fig. 4 G: ; ftEBR1::FLAG (1-1)/ftfd,ykiB5

Fig. S4. H and J: ; ftΔE::FLAG (5-2)/ftfd,ykiB5

Fig. S4 I: ; ftEBR1/2::FLAG (4-3)/ftfd,ykiB5

Fig. S4, B and B′ and Fig. 5, A and A′, D and D′, G and G′: hsFLP; ubi-mRFP.nls, FRT40A/ftEBR1::FLAG (1-1), FRT40A

Fig. S4, C and C′ and Fig. 5, B, B′, E, E′, H, and H′: hsFLP; ubi-mRFP.nls, FRT40A/ftΔE::FLAG (5-2), FRT40A

Fig. S4, D and D′, Fig. 5, C and C′, F and F′, I and I′: hsFLP; ubi-mRFP.nls, FRT40A/ftEBR1/2::FLAG (4-3), FRT40A

Fig. S4 A (lane1), E: ; ft::FLAG (2)/ft::FLAG (5)

Fig. S4 A (lane2), F: ; ftEBR1::FLAG (1-1)/ftEBR1::FLAG (3-2)

Fig. S4 A (lane3), G: ; ftΔE::FLAG (1–2)/ftΔE::FLAG (5-2)

Fig. S4 A (lane4), H-I: ; ftEBR1/2::FLAG (1–5)/ftEBR1/2::FLAG (4-3)

Fig. 5, J and K′, Fig. S5, E–I′: hsFLP; ubi-mRFP.nls, FRT40A/ds38k, FRT40A

Fig. S5, C and C′; UAS-Dicer2/UAS-fbxl7IR (BL60461); en-Gal4, UAS-GFP/+

Fig. S5, D and D′: ; UAS-fbxl7IR (BL60461)/+; hh-Gal4, ubi-Ex1-468::GFP/+

Immunostaining

Imaginal discs were dissected, fixed using 4% formaldehyde (Thermo Fisher Scientific) for 20 min and stained as per standard protocols. Primary antibodies were incubated overnight at 4°C and secondary antibodies were incubated for 1–2 h at room temperature. Tissue was incubated with Hoechst 33,342 (Thermo Fisher Scientific) for 5 min and mounted in ProLong Diamond Antifade (Thermo Fisher Scientific). Imaging was performed on a Nikon Ti2 confocal laser scanning microscope, using either the 100× Plan Apo 100 objective or the 60× Apo

objective, both with a numerical aperture of 1.4. Images were captured at room temperature. XY confocal micrographs of third instar wing imaginal discs represent max-intensity projections of apical z-stacks merged with single sections at the nuclei. Primary antibodies: rat anti-Ci155 (2A1; Developmental Studies Hybridoma Bank [DSHB]), mouse anti-Crb 1:50 (Cq4; DSHB)—post-fixed tissue serially dehydrated with 30, 50, and 70% methanol, rat anti-Crb 1:200 (kindly provided by F. Pichaud, University College London, London, UK), rabbit anti-Ds 1:200 (DZ41169; Boster Biological Technology), rat anti-Dachs 1:1000, rabbit anti-Dlish 1:100—preabsorbed with fixed *dlish*^{B1601} homozygous mutant larvae (both kindly provided by S. Blair), guinea pig anti-Ex 1:1,000—preabsorbed with fixed *ex*^{e1} homozygous mutant larvae (kindly provided by R. Fehon, University of Chicago, Chicago, IL, USA), rat anti-Ft 1:500 (Sopko et al., 2009), and rat anti-HA 1:250 (3F10; Roche Applied Science). Secondary antibodies used 1:1000: goat anti-guinea pig Alexa Fluor 488, goat anti-guinea pig Alexa Fluor 647, donkey anti-mouse Alexa Fluro 488, donkey anti-rabbit Alexa Fluro 488, donkey anti-rat Alexa Fluor 594, and donkey anti-rat Alexa Fluor 647 (all Thermo Fisher Scientific).

Cell culture, transfection, and expression construct generation

Drosophila S2R$^+$ cells were cultured at 25°C in Schneider's S2 media (Thermo Fisher Scientific) supplemented with 10% FBS (Sigma-Aldrich), 100 µ/ml penicillin and 100 µg/ml streptomycin (Thermo Fisher Scientific). DNA was transfected using the Effectene reagent (Qiagen). HEK293 cells were cultured at 37°C and 5% CO_2 in DMEM (Thermo Fisher Scientific) supplemented with 10% FBS (Sigma-Aldrich), 1% GlutaMAX (Thermo Fisher Scientific), 100 µ/ml penicillin, and 100 µg/ml streptomycin (Thermo Fisher Scientific). DNA was transfected using the Lipofectamine 2000 (Thermo Fisher Scientific) or Lipofectamine 3000 reagents (Thermo Fisher Scientific).

Cloning into cell expression vectors was performed us using standard PCR/restriction enzyme-based cloning, Gateway technology (Thermo Fisher Scientific), Q5 Site-Directed Mutagenesis (New England BioLabs), or the pCDNA3.1/V5-His TOPO TA Expression Kit (Thermo Fisher Scientific) and confirmed by sequencing.

Expression constructs

pAWF Ex^{FL} and pAWF Ex^{FERM} (FERM domain defined as amino acids 1–400; Badouel et al., 2009) and pAc Ft$^{\Delta ECD}$ (Matakatsu and Blair, 2006).

pCMV5 Ft$^{\Delta ECD}$::FLAG (Sopko et al., 2009) was used to subclone all pCMV5 Ft$^{\Delta ECD}$::FLAG constructs described below, using methods described above. All vectors were verified by sequencing. For constructs made for this study and primer pairs, see Table S1.

Lysate preparation and IP

S2R$^+$ lysates were generated using lysis buffer: 50 mM Tris, pH 7.5, 150 mM NaCl, 1% Triton X-100, 10% glycerol, and 1 mM EDTA supplemented with HALT protease and phosphatase inhibitor cocktail (Thermo Fisher Scientific). HEK293 lysates were generated using lysis buffer: 50 mM Hepes, 100 mM KCl, 2 mM EDTA, 0.1% NP40 (IGEPAL CA-630) and 10% glycerol supplemented with HALT protease and phosphatase inhibitor cocktail (Thermo Fisher Scientific). *Drosophila* L3 larval wing disc lysates were generated using 2× Laemmli buffer (Bio-Rad). FLAG-immunopurification was performed by incubating cell extract with anti-FLAG M2 affinity agarose gel (Sigma-Aldrich) for ≥2 h at 4°C under agitation. FLAG beads were subsequently washed with lysis buffer and eluted by incubation with 2× SDS sample buffer for 4 min at 95°C or by elution using 150 ng/µl FLAG peptide (Sigma-Aldrich) for 30–60 min.

Immunoblotting

Lysates were analyzed by standard chemiluminescent immunoblotting techniques. Primary antibodies: mouse anti-actin 1:2000 (C-4; Sigma-Aldrich), mouse anti-biotin 1:400 (33; Santa Cruz Biotechnology), rat anti-Ft 1:500 (Sopko et al., 2009), mouse anti-FLAG 1:5,000 (M2; Sigma-Aldrich), mouse anti-GST 1:500 (B-14; Santa Cruz Biotechnology), rabbit anti-HA 1:1,000 (C29F4; Cell Signaling Technology), rat anti-HA 1:2,000 (3F10; Roche Applied Science), and mouse anti-V5 1:5,000 (R960-25; Thermo Fisher Scientific).

PLA

PLA was performed using the Duolink kit (Sigma-Aldrich) as per manufacturer's protocol. Wing discs were incubated with PLA probes for 2 h at 37°C, ligase for 1 h at 37°C, and polymerase for 2 h at 37°C. Samples were stained with Hoechst 33,342 (Thermo Fisher Scientific) and mounted in ProLong Diamond Antifade (Thermo Fisher Scientific). Primary antibodies: mouse anti-FLAG 1:250 (M2; Sigma-Aldrich), rabbit anti-GFP 1:1,000 (ab290; Abcam).

GST expression and purification

GST-proteins were transformed into Rosetta (DE3) cells (Sigma-Aldrich) and induced by incubation with 0.1 mM Isopropyl ß-D-1-thiogalactopyranoside at 18°C. Bacteria were lysed using B-PER Complete (Thermo Fisher Scientific) supplemented with HALT protease and phosphatase inhibitor cocktail (Thermo Fisher Scientific) and GST-tagged protein was isolated using Glutathione Sepharose (Sigma-Aldrich) and eluted using 10 mM reduced glutathione, 50 mM Tris-HCl, pH 8. Buffer exchange into PBS was performed using Zeba Spin Desalting Columns (Thermo Fisher Scientific).

Binding assay between GST, biotin-tagged, or FLAG-tagged and in vitro translated protein

In vitro Dlish, GFP, Ex$^{1-468}$, Ex^{NT}, Ex^{CT}, and Ds^{ICD} were generated using TnT T7 Quick Coupled Transcription/Translation System (Promega) as per the manufacturer's protocol. N-terminally biotin-tagged Ft peptide was generated by GenScript. 100 pmol purified GST-protein, 10 µg biotin-peptide, or 10 µl FLAG-tagged TnT T7 product was incubated with 10 µl TnT T7 product in a total of 300 µl binding buffer: 0.02% NP40 (IGEPAL CA-630), 10% glycerol, PBS supplemented with 0.5 mM DTT, 0.1 mM PMSF, and HALT protease and phosphatase inhibitor cocktail (Thermo Fisher Scientific) for 2 h at 4°C. GST-protein binding reactions were then incubated with Glutathione Sepharose

(Sigma-Aldrich) and biotin-peptide binding reactions were incubated with Pierce Streptavidin Agarose (Thermo Fisher Scientific) for 2 h at 4°C before purification by centrifugation. Beads were washed with PBS and were eluted by incubation with 2× Laemmli, 5% 2-Mercaptoethanol at 95°C for 8 min. FLAG-binding reactions were incubated with anti-FLAG M2 affinity agarose gel (Sigma-Aldrich) overnight at 4°C before purification by centrifugation. Beads were washed with PBS and eluted by incubation with 150 ng/µl FLAG peptide (Sigma-Aldrich) for 30–60 min. 2× SDS sample buffer was added to supernatant and incubated for 5 min at 95°C. Binding was analyzed by immunoblotting.

Pupal lethality analysis

The percentage of pupal lethality was calculated by counting the total number of pupal cases and the number of non-eclosed pupal cases from the same vials and presented as a ratio. Statistical analysis by one-way ANOVA with the Dunnett's post-hoc test was performed in GraphPad Prism. Data distribution was assumed to be normal.

Adult wing analysis

Adult *Drosophila* were collected in 70% ethanol. Wings were removed in isopropanol, mounted in Euparal (Anglian Lepidopterist Suppliers), and baked at 65°C for ≥5 h. Imaging was performed using a Leica M165 FC stereo microscope, using a 1× Plan Apo objective with a numerical aperture of 0.81. Images captured using the Leica DMC 4500 camera at room temperature. Wing parameters were quantified using ImageJ. The L3 vein was used to calculate wing length, and the distance between the distal ends of the L2 and L5 veins was used to calculate wing width, which were presented as a ratio to measure shape. Statistical analysis by one-way ANOVA with the Tukey's or Dunnett's post-hoc test was performed in GraphPad Prism. Data distribution was assumed to be normal.

Immunofluorescence quantification and processing

For quantification of apical fluorescence inside vs. outside a clone, regions of interest were manually defined using the fluorescent clonal marker. Apical or basal mean pixel intensity was measured using NIS-Elements (Nikon) or ImageJ. Data points represent the averaged signals from at least two transverse sections per wing disc normalized to the average signal from the wild-type tissue. Statistical analysis by unpaired t-test or one-way ANOVA with the Tukey's post-hoc test was performed in GraphPad Prism. Data distribution was assumed to be normal. Where indicated, images were denoised using NIS-Elements (Nikon).

Online supplemental material

Fig. S1 presents further data showing Ft and Crb regulate Ex independently. Fig. S2 presents additional data showing Ft and Ex colocalization and interaction. Fig. S3 shows additional data identifying EBRs. Fig. S4 provides more data showing the EBRs are required in vivo for regulation of tissue growth. Fig. S5 shows additional in vivo data and binding data showing Ds does not directly bind Ex or Dlish. Table S1 shows DNA constructs and primers made for this study.

Acknowledgments

We thank S. Blair, R. Fehon, and F. Pichaud for flies and/or reagents. We are grateful to members of the McNeill lab for helpful discussion and P.S. Ribeiro for critically reading the manuscript. Stocks obtained from the Bloomington Drosophila Stock Center (National Institutes of Health [NIH] P40OD018537) were used in this study. The antibodies Ci (2A1) and Crb (Cq4) were obtained from the DSHB, created by the National Institute of Child Health and Human Development of the NIH and maintained at The University of Iowa, Department of Biology, Iowa City, IA, USA.

Work in the McNeill lab was funded by NIH RO1 GM138853 and BJC investigator support. M.V. Holder and N. Tapon were supported by the Francis Crick Institute, which receives its core funding from Cancer Research UK (CC2138), the UK Medical Research Council (CC2138), and the Wellcome Trust (CC2138). This research was funded in part by the Wellcome Trust [Grant number CC2138]. For the purpose of Open Access, the authors have applied a CC BY public copyright license to any Author Accepted Manuscript version arising from this submission..

Authors contributions: A.D. Fulford, L. Enderle, and H. McNeill conceptualized the experiments. A.D. Fulford, L. Enderle, J. Rusch, D. Hodzic, M.V. Holder, A. Earl, and R.H. Oh performed the experiments. N. Tapon read and edited the manuscript. A.D. Fulford and H. McNeill wrote the manuscript, which was read and edited by all authors.

Disclosures: The authors declare no competing interests exist.

Submitted: 23 May 2022
Revised: 26 November 2022
Accepted: 9 February 2023

References

Alam, M.S. 2018. Proximity ligation assay (PLA). *Curr. Protoc. Immunol.* 123: e58. https://doi.org/10.1002/cpim.58

Badouel, C., L. Gardano, N. Amin, A. Garg, R. Rosenfeld, T. Le Bihan, and H. McNeill. 2009. The FERM-domain protein Expanded regulates Hippo pathway activity via direct interactions with the transcriptional activator Yorkie. *Dev. Cell.* 16:411–420. https://doi.org/10.1016/j.devcel.2009.01.010

Baumgartner, R., I. Poernbacher, N. Buser, E. Hafen, and H. Stocker. 2010. The WW domain protein Kibra acts upstream of Hippo in Drosophila. *Dev. Cell.* 18:309–316. https://doi.org/10.1016/j.devcel.2009.12.013

Bennett, F.C., and K.F. Harvey. 2006. Fat cadherin modulates organ size in Drosophila via the Salvador/Warts/Hippo signaling pathway. *Curr. Biol.* 16:2101–2110. https://doi.org/10.1016/j.cub.2006.09.045

Blair, S., and H. McNeill. 2018. Big roles for Fat cadherins. *Curr. Opin. Cell Biol.* 51:73–80. https://doi.org/10.1016/j.ceb.2017.11.006

Boggiano, J.C., P.J. Vanderzalm, and R.G. Fehon. 2011. Tao-1 phosphorylates Hippo/MST kinases to regulate the Hippo-Salvador-Warts tumor suppressor pathway. *Dev. Cell.* 21:888–895. https://doi.org/10.1016/j.devcel.2011.08.028

Bosch, J.A., T.M. Sumabat, Y. Hafezi, B.J. Pellock, K.D. Gandhi, and I.K. Hariharan. 2014. The Drosophila F-box protein Fbxl7 binds to the protocadherin fat and regulates Dachs localization and Hippo signaling. *Elife.* 3:e03383. https://doi.org/10.7554/eLife.03383

Bossuyt, W., C.-L. Chen, Q. Chen, M. Sudol, H. McNeill, D. Pan, A. Kopp, and G. Halder. 2014. An evolutionary shift in the regulation of the Hippo pathway between mice and flies. *Oncogene.* 33:1218–1228. https://doi.org/10.1038/onc.2013.82

Bosveld, F., I. Bonnet, B. Guirao, S. Tlili, Z. Wang, A. Petitalot, R. Marchand, P.-L. Bardet, P. Marcq, F. Graner, and Y. Bellaïche. 2012. Mechanical control of morphogenesis by Fat/Dachsous/Four-jointed planar cell

polarity pathway. *Science*. 336:724–727. https://doi.org/10.1126/science.1221071

Brittle, A.L., A. Repiso, J. Casal, P.A. Lawrence, and D. Strutt. 2010. Four-jointed modulates growth and planar polarity by reducing the affinity of dachsous for fat. *Curr. Biol.* 20:803–810. https://doi.org/10.1016/j.cub.2010.03.056

Brittle, A., C. Thomas, and D. Strutt. 2012. Planar polarity specification through asymmetric subcellular localization of Fat and Dachsous. *Curr. Biol.* 22:907–914. https://doi.org/10.1016/j.cub.2012.03.053

Chen, C.-L., K.M. Gajewski, F. Hamaratoglu, W. Bossuyt, L. Sansores-Garcia, C. Tao, and G. Halder. 2010. The apical-basal cell polarity determinant Crumbs regulates Hippo signaling in Drosophila. *Proc. Natl. Acad. Sci. USA*. 107:15810–15815. https://doi.org/10.1073/pnas.1004060107

Cho, E., Y. Feng, C. Rauskolb, S. Maitra, R. Fehon, and K.D. Irvine. 2006. Delineation of a Fat tumor suppressor pathway. *Nat. Genet.* 38:1142–1150. https://doi.org/10.1038/ng1887

Chung, H.-L., G.J. Augustine, and K.-W. Choi. 2016. Drosophila Schip1 links expanded and Tao-1 to regulate hippo signaling. *Dev. Cell*. 36:511–524. https://doi.org/10.1016/j.devcel.2016.02.004

Degoutin, J.L., C.C. Milton, E. Yu, M. Tipping, F. Bosveld, L. Yang, Y. Bellaiche, A. Veraksa, and K.F. Harvey. 2013. Riquiqui and minibrain are regulators of the hippo pathway downstream of Dachsous. *Nat. Cell Biol.* 15:1176–1185. https://doi.org/10.1038/ncb2829

Feng, Y., and K.D. Irvine. 2009. Processing and phosphorylation of the Fat receptor. *Proc. Natl. Acad. Sci. USA*. 106:11989–11994. https://doi.org/10.1073/pnas.0811540106

Fulford, A.D., M.V. Holder, D. Frith, A.P. Snijders, N. Tapon, and P.S. Ribeiro. 2019. Casein kinase 1 family proteins promote Slimb-dependent Expanded degradation. *Elife*. 8:e46592. https://doi.org/10.7554/eLife.46592

Fletcher, G.C., A. Elbediwy, I. Khanal, P.S. Ribeiro, N. Tapon, and B.J. Thompson. 2015. The Spectrin cytoskeleton regulates the Hippo signalling pathway. *EMBO J.* 34(7):940–954. https://doi.org/10.15252/embj.201489642

Fulford, A.D., and H. McNeill. 2020. Fat/Dachsous family cadherins in cell and tissue organisation. *Curr. Opin. Cell Biol.* 62:96–103. https://doi.org/10.1016/j.ceb.2019.10.006

Fulford, A., N. Tapon, and P.S. Ribeiro. 2018. Upstairs, downstairs: Spatial regulation of hippo signalling. *Curr. Opin. Cell Biol.* 51:22–32. https://doi.org/10.1016/j.ceb.2017.10.006

Genevet, A., and N. Tapon. 2011. The Hippo pathway and apico-basal cell polarity. *Biochem. J.* 436:213–224. https://doi.org/10.1042/BJ20110217

Genevet, A., M.C. Wehr, R. Brain, B.J. Thompson, and N. Tapon. 2010. Kibra is a regulator of the Salvador/Warts/Hippo signaling network. *Dev. Cell*. 18:300–308. https://doi.org/10.1016/j.devcel.2009.12.011

Grzeschik, N.A., L.M. Parsons, M.L. Allott, K.F. Harvey, and H.E. Richardson. 2010. Lgl, aPKC, and Crumbs regulate the Salvador/Warts/Hippo pathway through two distinct mechanisms. *Curr. Biol.* 20:573–581. https://doi.org/10.1016/j.cub.2010.01.055

Gunn-Moore, F.J., M. Hill, F. Davey, L.R. Herron, S. Tait, D. Sherman, and P.J. Brophy. 2006. A functional FERM domain binding motif in neurofascin. *Mol. Cell. Neurosci.* 33:441–446. https://doi.org/10.1016/j.mcn.2006.09.003

Hale, R., A.L. Brittle, K.H. Fisher, N.A.M. Monk, and D. Strutt. 2015. Cellular interpretation of the long-range gradient of Four-jointed activity in the Drosophila wing. *Elife*. 4:e05789. https://doi.org/10.7554/eLife.05789

Hamaratoglu, F., M. Willecke, M. Kango-Singh, R. Nolo, E. Hyun, C. Tao, H. Jafar-Nejad, and G. Halder. 2006. The tumour-suppressor genes NF2/Merlin and Expanded act through Hippo signalling to regulate cell proliferation and apoptosis. *Nat. Cell Biol.* 8:27–36. https://doi.org/10.1038/ncb1339

Harvey, K.F., C.M. Pfleger, and I.K. Hariharan. 2003. The Drosophila Mst ortholog, hippo, restricts growth and cell proliferation and promotes apoptosis. *Cell*. 114:457–467. https://doi.org/10.1016/s0092-8674(03)00557-9

Hu, L., J. Xu, M.-X. Yin, L. Zhang, Y. Lu, W. Wu, Z. Xue, M.S. Ho, G. Gao, Y. Zhao, and L. Zhang. 2016. Ack promotes tissue growth via phosphorylation and suppression of the Hippo pathway component Expanded. *Cell Discov.* 2:15047. https://doi.org/10.1038/celldisc.2015.47

Huang, J., S. Wu, J. Barrera, K. Matthews, and D. Pan. 2005. The Hippo signaling pathway coordinately regulates cell proliferation and apoptosis by inactivating Yorkie, the Drosophila Homolog of YAP. *Cell*. 122:421–434. https://doi.org/10.1016/j.cell.2005.06.007

Irvine, K.D., and K.F. Harvey. 2015. Control of organ growth by patterning and hippo signaling in Drosophila. *Cold Spring Harb. Perspect. Biol.* 7:a019224. https://doi.org/10.1101/cshperspect.a019224

Ishikawa, H.O., H. Takeuchi, R.S. Haltiwanger, and K.D. Irvine. 2008. Four-jointed is a Golgi kinase that phosphorylates a subset of cadherin domains. *Science*. 321:401–404. https://doi.org/10.1126/science.1158159

Jia, J., W. Zhang, B. Wang, R. Trinko, and J. Jiang. 2003. The Drosophila Ste20 family kinase dMST functions as a tumor suppressor by restricting cell proliferation and promoting apoptosis. *Genes Dev.* 17:2514–2519. https://doi.org/10.1101/gad.1134003

Justice, R.W., O. Zilian, D.F. Woods, M. Noll, and P.J. Bryant. 1995. The Drosophila tumor suppressor gene warts encodes a homolog of human myotonic dystrophy kinase and is required for the control of cell shape and proliferation. *Genes Dev.* 9:534–546. https://doi.org/10.1101/gad.9.5.534

Ling, C., Y. Zheng, F. Yin, J. Yu, J. Huang, Y. Hong, S. Wu, and D. Pan. 2010. The apical transmembrane protein Crumbs functions as a tumor suppressor that regulates Hippo signaling by binding to Expanded. *Proc. Natl. Acad. Sci. USA*. 107:10532–10537. https://doi.org/10.1073/pnas.1004279107

Ma, D., C.H. Yang, H. McNeill, M.A. Simon, and J.D. Axelrod. 2003. Fidelity in planar cell polarity signalling. *Nature*. 421:543–547. https://doi.org/10.1038/nature01366

Ma, X., X. Guo, H.E. Richardson, T. Xu, and L. Xue. (2018). POSH regulates Hippo signaling through ubiquitin-mediated expanded degradation. *Proc. Natl. Acad. Sci.* 115:2150 LP–2155. https://doi.org/10.1073/pnas.1715165115

Mao, Y., B. Kucuk, and K.D. Irvine. 2009. Drosophila lowfat, a novel modulator of Fat signaling. *Development*. 136:3223–3233. https://doi.org/10.1242/dev.036152

Mao, Y., C. Rauskolb, E. Cho, W.-L. Hu, H. Hayter, G. Minihan, F.N. Katz, and K.D. Irvine. 2006. Dachs: An unconventional myosin that functions downstream of fat to regulate growth, affinity and gene expression in Drosophila. *Development*. 133:2539–2551. https://doi.org/10.1242/dev.02427

Matakatsu, H., and S.S. Blair. 2004. Interactions between Fat and Dachsous and the regulation of planar cell polarity in the Drosophila wing. *Development*. 131:3785–3794. https://doi.org/10.1242/dev.01254

Matakatsu, H., and S.S. Blair. 2006. Separating the adhesive and signaling functions of the Fat and Dachsous protocadherins. *Development*. 133:2315–2324. https://doi.org/10.1242/dev.02401

Matakatsu, H., and S.S. Blair. 2008. The DHHC palmitoyltransferase approximated regulates Fat signaling and Dachs localization and activity. *Curr. Biol.* 18:1390–1395. https://doi.org/10.1016/j.cub.2008.07.067

Matakatsu, H., and S.S. Blair. 2012. Separating planar cell polarity and Hippo pathway activities of the protocadherins Fat and Dachsous. *Development*. 139:1498–1508. https://doi.org/10.1242/dev.070367

Matakatsu, H., S.S. Blair, and R.G. Fehon. 2017. The palmitoyltransferase Approximated promotes growth via the Hippo pathway by palmitoylation of Fat. *J. Cell Biol.* 216:265–277. https://doi.org/10.1083/jcb.201609094

McCartney, B.M., R.M. Kulikauskas, D.R. LaJeunesse, and R.G. Fehon. 2000. The neurofibromatosis-2 homologue, Merlin, and the tumor suppressor expanded function together in Drosophila to regulate cell proliferation and differentiation. *Development*. 127:1315–1324. https://doi.org/10.1242/dev.127.6.1315

Misra, J.R., and K.D. Irvine. 2016. Vamana couples fat signaling to the hippo pathway. *Dev. Cell*. 39:254–266. https://doi.org/10.1016/j.devcel.2016.09.017

Misra, J.R., and K.D. Irvine. 2018. The hippo signaling network and its biological functions. *Annu. Rev. Genet.* 52:65–87. https://doi.org/10.1146/annurev-genet-120417-031621

Oh, H., B.V.V.G. Reddy, and K.D. Irvine. 2009. Phosphorylation-independent repression of Yorkie in fat-hippo signaling. *Dev. Biol.* 335:188–197. https://doi.org/10.1016/j.ydbio.2009.08.026

Pan, G., Y. Feng, A.A. Ambegaonkar, G. Sun, M. Huff, C. Rauskolb, and K.D. Irvine. 2013. Signal transduction by the Fat cytoplasmic domain. *Development*. 140:831–842. https://doi.org/10.1242/dev.088534

Pantalacci, S., N. Tapon, and P. Léopold. 2003. The Salvador partner Hippo promotes apoptosis and cell-cycle exit in Drosophila. *Nat. Cell Biol.* 5:921–927. https://doi.org/10.1038/ncb1051

Poon, C.L.C., J.I. Lin, X. Zhang, and K.F. Harvey. 2011. The sterile 20-like kinase Tao-1 controls tissue growth by regulating the Salvador-Warts-Hippo pathway. *Dev. Cell*. 21:896–906. https://doi.org/10.1016/j.devcel.2011.09.012

Ragni, C.V., N. Diguet, J.F. Le Garrec, M. Novotova, T.P. Resende, S. Pop, N. Charon, L. Guillemot, L. Kitasato, C. Badouel, et al. 2017. Amotl1 mediates sequestration of the Hippo effector Yap1 downstream of Fat4 to

restrict heart growth. *Nat. Commun.* 8:14582. https://doi.org/10.1038/ncomms14582

Rauskolb, C., G. Pan, B.V.V.G. Reddy, H. Oh, and K.D. Irvine. 2011. Zyxin links fat signaling to the hippo pathway. *PLoS Biol.* 9:e1000624. https://doi.org/10.1371/journal.pbio.1000624

Ribeiro, P., M. Holder, D. Frith, A.P. Snijders, and N. Tapon. 2014. Crumbs promotes expanded recognition and degradation by the SCF(Slimb/β-TrCP) ubiquitin ligase. *Proc. Natl. Acad. Sci. USA.* 111:E1980–E1989. https://doi.org/10.1073/pnas.1315508111

Robinson, B.S., J. Huang, Y. Hong, and K.H. Moberg. 2010. Crumbs regulates Salvador/Warts/Hippo signaling in Drosophila via the FERM-domain protein Expanded. *Curr. Biol.* 20:582–590. https://doi.org/10.1016/j.cub.2010.03.019

Rodrigues-Campos, M., and B.J. Thompson. 2014. The ubiquitin ligase FbxL7 regulates the Dachsous-Fat-Dachs system in Drosophila. *Development.* 141:4098–4103. https://doi.org/10.1242/dev.113498

Sharma, P., and H. McNeill. 2013. Regulation of long-range planar cell polarity by Fat-Dachsous signaling. *Development.* 140:3869–3881. https://doi.org/10.1242/dev.094730

Silva, E., Y. Tsatskis, L. Gardano, N. Tapon, and H. McNeill. 2006. The tumor-suppressor gene fat controls tissue growth upstream of expanded in the hippo signaling pathway. *Curr. Biol.* 16:2081–2089. https://doi.org/10.1016/j.cub.2006.09.004

Simon, M.A., A. Xu, H.O. Ishikawa, and K.D. Irvine. 2010. Modulation of fat: dachsous binding by the cadherin domain kinase four-jointed. *Curr. Biol.* 20:811–817. https://doi.org/10.1016/j.cub.2010.04.016

Sopko, R., E. Silva, L. Clayton, L. Gardano, M. Barrios-Rodiles, J. Wrana, X. Varelas, N.I. Arbouzova, S. Shaw, S. Saburi, et al. 2009. Phosphorylation of the tumor suppressor fat is regulated by its ligand Dachsous and the kinase discs overgrown. *Curr. Biol.* 19:1112–1117. https://doi.org/10.1016/j.cub.2009.05.049

Strutt, H., and D. Strutt. 2021. How do the Fat-Dachsous and core planar polarity pathways act together and independently to coordinate polarized cell behaviours?. *Open Biol.* 11:200356. https://doi.org/10.1098/rsob.200356

Su, T., M.Z. Ludwig, J. Xu, and R.G. Fehon. 2017. Kibra and Merlin activate the hippo pathway spatially distinct from and independent of expanded. *Dev. Cell.* 40:478–490.e3. https://doi.org/10.1016/j.devcel.2017.02.004

Sun, S., B.V.V.G. Reddy, and K.D. Irvine. 2015. Localization of Hippo signalling complexes and Warts activation in vivo. *Nat. Commun.* 6:8402. https://doi.org/10.1038/ncomms9402

Udan, R.S., M. Kango-Singh, R. Nolo, C. Tao, and G. Halder. 2003. Hippo promotes proliferation arrest and apoptosis in the Salvador/Warts pathway. *Nat. Cell Biol.* 5:914–920. https://doi.org/10.1038/ncb1050

Varelas, X., P. Samavarchi-Tehrani, M. Narimatsu, A. Weiss, K. Cockburn, B.G. Larsen, J. Rossant, and J.L. Wrana. 2010. The Crumbs complex couples cell density sensing to Hippo-dependent control of the TGF-β-SMAD pathway. *Dev. Cell.* 19:831–844. https://doi.org/10.1016/j.devcel.2010.11.012

Vrabioiu, A.M., and G. Struhl. 2015. Fat/Dachsous signaling promotes Drosophila wing growth by regulating the conformational state of the NDR kinase warts. *Dev. Cell.* 35:737–749. https://doi.org/10.1016/j.devcel.2015.11.027

Wang, X., Y. Zhang, and S.S. Blair. 2019. Fat-regulated adaptor protein Dlish binds the growth suppressor Expanded and controls its stability and ubiquitination. *Proc. Natl. Acad. Sci. USA.* 116:1319–1324. https://doi.org/10.1073/pnas.1811891116

Wu, S., J. Huang, J. Dong, and D. Pan. 2003. Hippo encodes a Ste-20 family protein kinase that restricts cell proliferation and promotes apoptosis in conjunction with salvador and warts. *Cell.* 114:445–456. https://doi.org/10.1016/s0092-8674(03)00549-x

Wu, S., Y. Liu, Y. Zheng, J. Dong, and D. Pan. 2008. The TEAD/TEF family protein Scalloped mediates transcriptional output of the Hippo growth-regulatory pathway. *Dev. Cell.* 14:388–398. https://doi.org/10.1016/j.devcel.2008.01.007

Xu, T., W. Wang, S. Zhang, R.A. Stewart, and W. Yu. 1995. Identifying tumor suppressors in genetic mosaics: The Drosophila lats gene encodes a putative protein kinase. *Development.* 121:1053–1063. https://doi.org/10.1242/dev.121.4.1053

Yu, J., Y. Zheng, J. Dong, S. Klusza, W.-M. Deng, and D. Pan. 2010. Kibra functions as a tumor suppressor protein that regulates Hippo signaling in conjunction with Merlin and Expanded. *Dev. Cell.* 18:288–299. https://doi.org/10.1016/j.devcel.2009.12.012

Zhang, H., C. Li, H. Chen, C. Wei, F. Dai, H. Wu, W. Dui, W.-M. Deng, and R. Jiao. 2015. SCF(Slmb) E3 ligase-mediated degradation of Expanded is inhibited by the Hippo pathway in Drosophila. *Cell Res.* 25:93–109. https://doi.org/10.1038/cr.2014.166

Zhang, L., F. Ren, Q. Zhang, Y. Chen, B. Wang, and J. Jiang. 2008. The TEAD/TEF family of transcription factor Scalloped mediates Hippo signaling in organ size control. *Dev. Cell.* 14:377–387. https://doi.org/10.1016/j.devcel.2008.01.006

Zhang, Y., X. Wang, H. Matakatsu, R. Fehon, and S.S. Blair. 2016. The novel SH3 domain protein Dlish/CG10933 mediates fat signaling in Drosophila by binding and regulating Dachs. *Elife.* 5:e16624. https://doi.org/10.7554/eLife.16624

Zhao, X., C.H. Yang, and M.A. Simon. 2013. The Drosophila Cadherin Fat regulates tissue size and planar cell polarity through different domains. *PLoS One.* 8:e62998. https://doi.org/10.1371/journal.pone.0062998

Zheng, Y., and D. Pan. 2019. The hippo signaling pathway in development and disease. *Dev. Cell.* 50:264–282. https://doi.org/10.1016/j.devcel.2019.06.003

Supplemental material

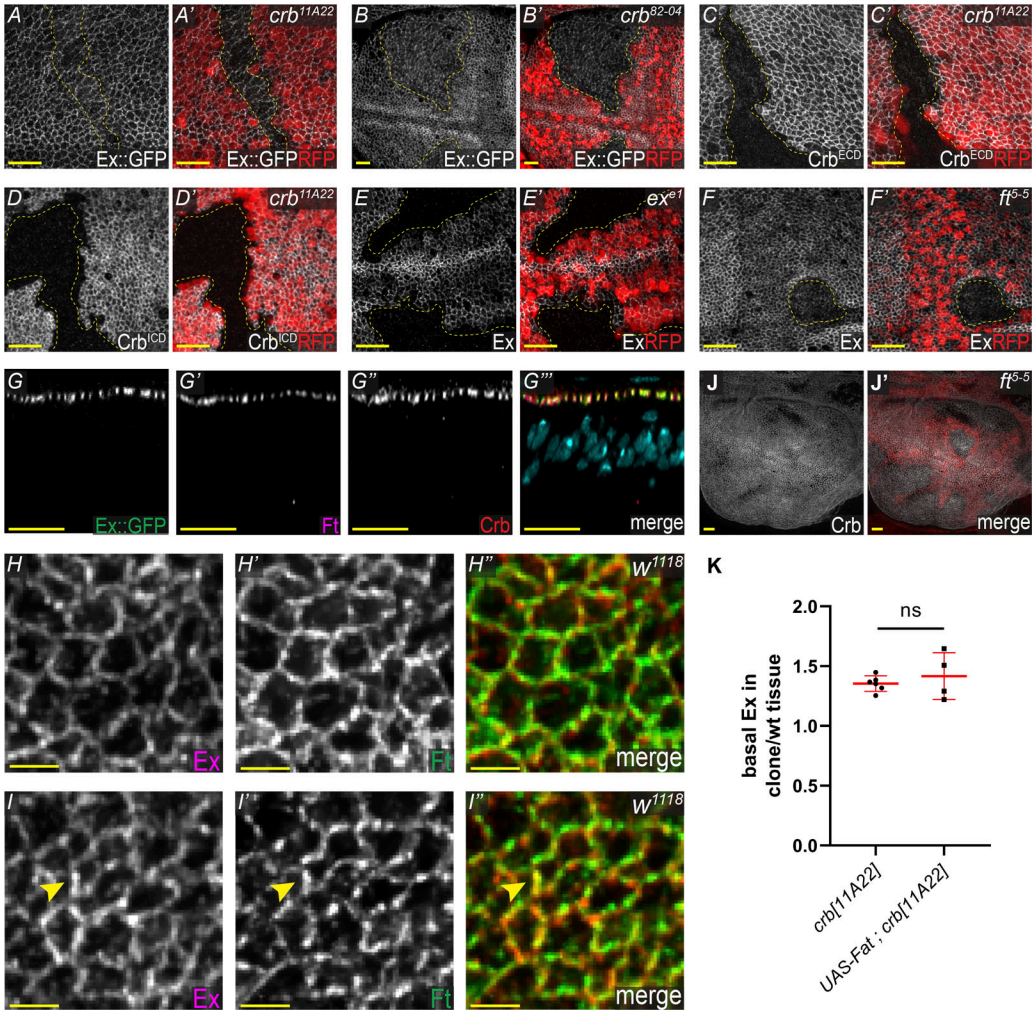

Figure S1. **Ft and Crb regulate Ex independently. (A–B′)** A portion of Ex::GFP remains at the apical membrane despite loss of Crb. XY confocal micrographs of Ex::GFP third instar wing imaginal discs containing *crb*^{11A22} (A and A′) or *crb*$^{82-04}$ (B and B′) mutant clones (marked by absence of RFP shown in red), showing direct GFP fluorescence representing Ex protein (shown in gray). **(C–D′)** Validation of *crb*^{11A22} as a protein null. XY confocal micrographs of third instar wing imaginal discs containing *crb*^{11A22} mutant clones (marked by absence of RFP shown in red) with immunostaining to the extracellular domain (ECD) of Crb (C and C′—shown in gray) or the ICD of Crb (D and D′—shown in grandy). **(E and E′)** Validation of Ex immunostaining. XY confocal micrographs of third instar wing imaginal discs containing *ex*^{e1} mutant clones (marked by absence of RFP shown in red) with Ex staining (shown in gray). **(F and F′)** Loss of Ft causes loss of apical Ex. XY confocal micrographs of third instar wing imaginal discs containing *ft*$^{5-5}$ mutant clones (marked by absence of RFP shown in red) with Ex staining (shown in gray). *ft*$^{5-5}$ is a remake of *ft*^{fd} and is a null allele. **(G–G‴)** Colocalization of Ex, Ft, and Crb at apical junctions. Transverse confocal micrograph of third instar wing imaginal discs with direct fluorescence of Ex::GFP (green in G and G‴), stained with Ft (mauve in G′ and G‴), Crb (red in G′′ and G‴), and Hoechst (cyan in merge) to mark nuclei. All images are orientated dorsal up. Clonal boundaries are marked by yellow dotted lines. Scale bars are 10 µm. **(H–I′′)** High-resolution localization patterns of Ex and Ft with even distribution (H–H′′) or punctate (I–I′′). High-resolution XY confocal micrographs of third instar wing imaginal discs stained for Ft (green in H′′ and I′′) and Ex (mauve in H′′ and I′′). The yellow arrowheads in I–I′′ highlight punctate colocalization. Images were denoised, scale bar is 2 µm. **(J and J′)** Loss of Ft does not affect Crb. XY confocal micrographs of third instar wing imaginal discs containing *ft*$^{5-5}$ mutant clones (marked by absence of RFP shown in red) with Crb staining (shown in gray). *ft*$^{5-5}$ is a remake of *ft*^{fd} and is a null allele. Images are oriented dorsal up. Scale bar is 10 µm. **(K)** Quantification of the ratio between basal Ex inside versus outside the MARCM clone normalized to the wild-type (wt) tissue. Data points represent an average of a single disc with the mean and SD indicated. No significance calculated using an unpaired *T* test.

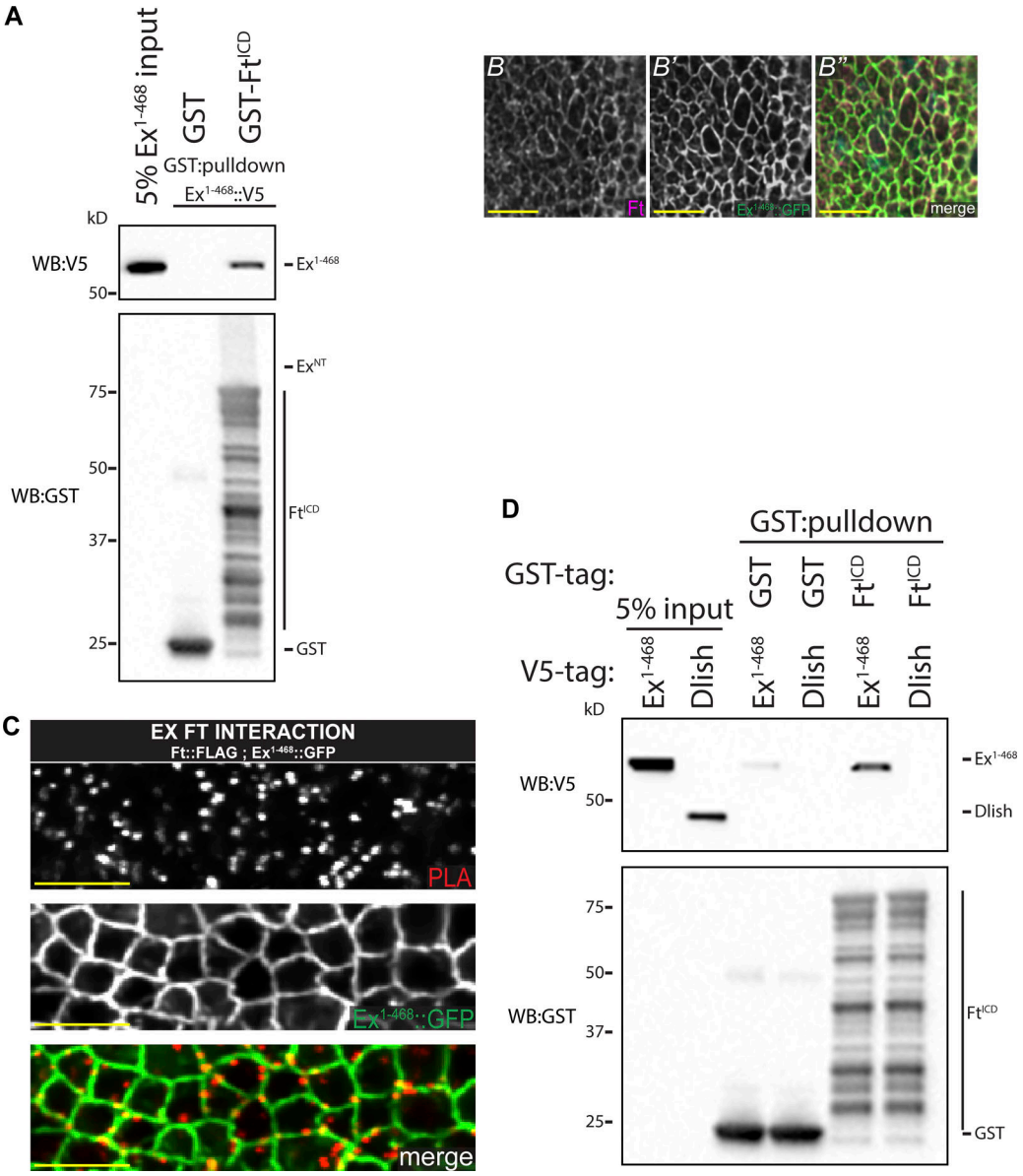

Figure S2. **Ft and Ex directly bind at the apical membrane. (A)** Ft^{ICD} directly binds Ex^{1-468}. In vitro transcribed and translated Ex^{1-468} was incubated with bacterially expressed and purified GST alone or GST::Ft^{ICD} and subjected to GST-purification. **(B–B′′)** High-resolution colocalization of Ex^{1-468} and Ft. XY confocal micrograph of third instar wing imaginal discs stained with Ft (mauve in B′′) with direct fluorescence of Ex^{1-468}::GFP (green in B′′). **(C)** Ft and Ex interact at apical membrane in vivo. XY confocal micrographs of third instar imaginal discs expressing *ubi-*Ex^{1-468}*::GFP* subjected to anti-FLAG and anti-GFP PLA. Ex::Ft interaction condition expresses *ft::FLAG* at the endogenous locus and *ubi-*Ex^{1-468}*::GFP*. Ex^{1-468}::GFP is observed by direct fluorescence of GFP (gray or green in merge), PLA signal (gray or red in merge) marks interaction loci, which overlap with Ex signal. Images were denoised, scale bar is 2 µm. **(D)** Ft^{ICD} does not directly binds Dlish. In vitro transcribed and translated Ex^{1-468} (as a positive control) and Dlish were incubated with bacterially expressed and purified GST alone or GST::Ft^{ICD} and subjected to GST-purification. The expression and presence of proteins was analyzed by immunoblotting with the indicated antibodies. WB, Western blot. Source data are available for this figure: SourceData FS2.

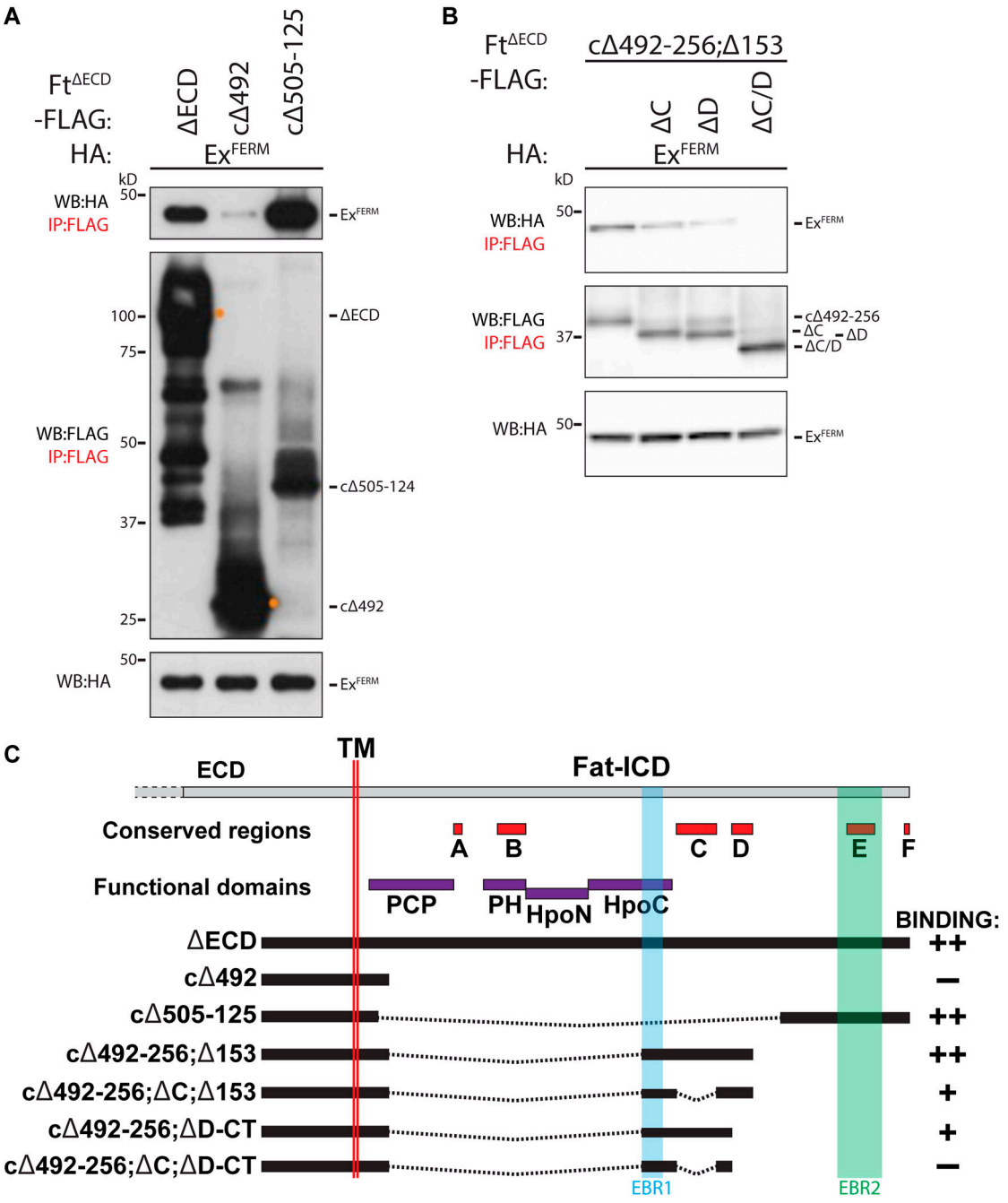

Figure S3. **Identification of EBRs within the Ft ICD. (A)** Identification of EBR2 in the Ft ICD. HEK293 cell expression and IP of indicated FLAG-tagged Ft$^{\Delta ECD}$ constructs in the presence of Ex^{FERM}. **(B)** Ft conserved C and D regions affect interaction with Ex. HEK293 cell expression and IP of indicated FLAG-tagged Ft$^{\Delta ECD}$ constructs in the presence of Ex^{FERM}. The expression and presence of proteins was analyzed by immunoblotting with the indicated antibodies. Ft presents as multiple bands due to proteolytic processing (Feng and Irvine, 2009; Sopko et al., 2009). **(C)** Graphical scheme highlighting the Ft constructs used in the figure. In addition, the transmembrane domain (TM), EBR1, EBR2, and established conserved and function domains of the Ft ICD are depicted. In binding column: "++" denotes constructs that interact strongly to Ex^{FERM}, "+" denotes weak interaction with Ex^{FERM}, and "–" denotes no interaction with Ex^{FERM}. WB, Western blot. Source data are available for this figure: SourceData FS3.

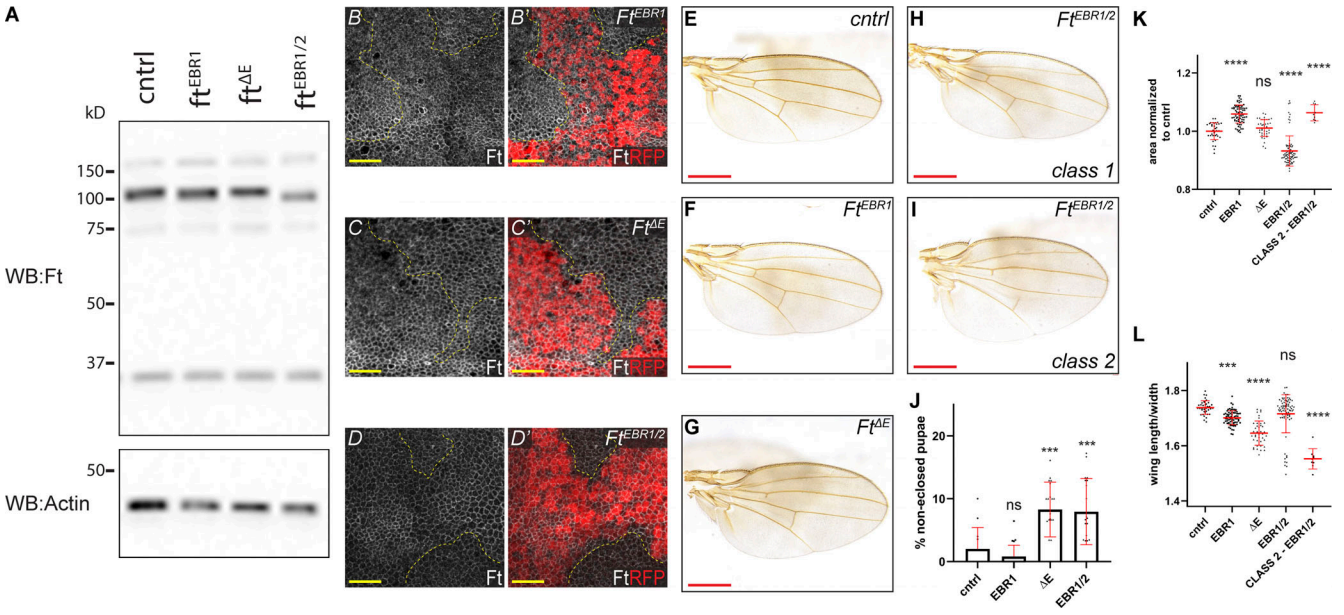

Figure S4. **EBRs are required in vivo for regulation of tissue growth. (A)** EBR deletion does not affect Ft levels. Immunoblot of trans-heterozygous EBR allele L3 wing discs. Compared to cntrl (ft::FLAG), there is no change in Ft levels in the EBR alleles. Proteins were analyzed by immunoblotting with the indicated antibodies. Actin was used as a loading control. Ft presents as multiple bands due to proteolytic processing (Feng and Irvine, 2009; Sopko et al., 2009). **(B–D′)** EBR deletion does not affect Ft levels or localization. XY confocal micrographs third instar wing imaginal discs containing of ft^{EBR1} (B and B′), $ft^{\Delta E}$ (C and C′), or $ft^{EBR1/2}$ (D and D′) mutant clones (marked by absence of RFP shown in red) with Ft staining (shown in gray). XY images are orientated as dorsal up. Clonal boundaries are marked by yellow dotted lines. Scale bars are 10 µm. **(E–I)** Effect of trans-heterozygous EBR deletion on adult wing phenotypes. Phenotype of control (cntrl)—ft::FLAG (E), ft^{EBR1} (F), $ft^{\Delta E}$ (G), bulk $ft^{EBR1/2}$ (class 1; H), or $ft^{EBR1/2}$ (class 2; I) wings. Scale bars are 500 µm. **(J)** Quantification of pupal lethality in trans-heterozygous EBR animals. Compared to cntrl (ft::FLAG) wings, $ft^{\Delta E}$ and $ft^{EBR1/2}$ cause a significant increase in pupal lethality. Data points indicate one vial of ∼30 pupae, with number of vials ≥10 per genotype, with mean and SD represented. ***P < 0.005 using one-way ANOVA with a Dunnett's post-hoc test compared to the ft::FLAG control. ns denotes non-significant. **(K)** Quantification of adult wing size in trans-heterozygous EBR flies. Data are normalized against the mean of the cntrl (ft::FLAG). ft^{EBR1} causes significant overgrowth. $ft^{EBR1/2}$ class 2 flies are isolated from the bulk $ft^{EBR1/2}$ to indicate the significant overgrowth. Data points indicate an individual wing (n ≥ 38 per genotype, class 2 flies n = 9), with mean and SD represented. ****P < 0.0001 using one-way ANOVA with a Dunnett's post-hoc test compared to cntrl. ns denotes non-significant. **(L)** Quantification of adult wing roundness in trans-heterozygous EBR flies. Shape was determined by the ratio of wing length verses width. Data are normalized against the mean of the cntrl (ft::FLAG). ft^{EBR1} and $ft^{\Delta E}$ are significantly rounder than cntrl. $ft^{EBR1/2}$ class 2 flies are isolated from the bulk $ft^{EBR1/2}$ to indicate the significant increase in roundness. Data points indicate an individual wing (n ≥ 38 per genotype, class 2 flies n = 9), with mean and SD represented. ***P = 0.0004 and ****P < 0.0001 using one-way ANOVA with a Dunnet's post-hoc test compared to cntrl. ns denotes non-significant. WB, Western blot. Source data are available for this figure: SourceData FS4.

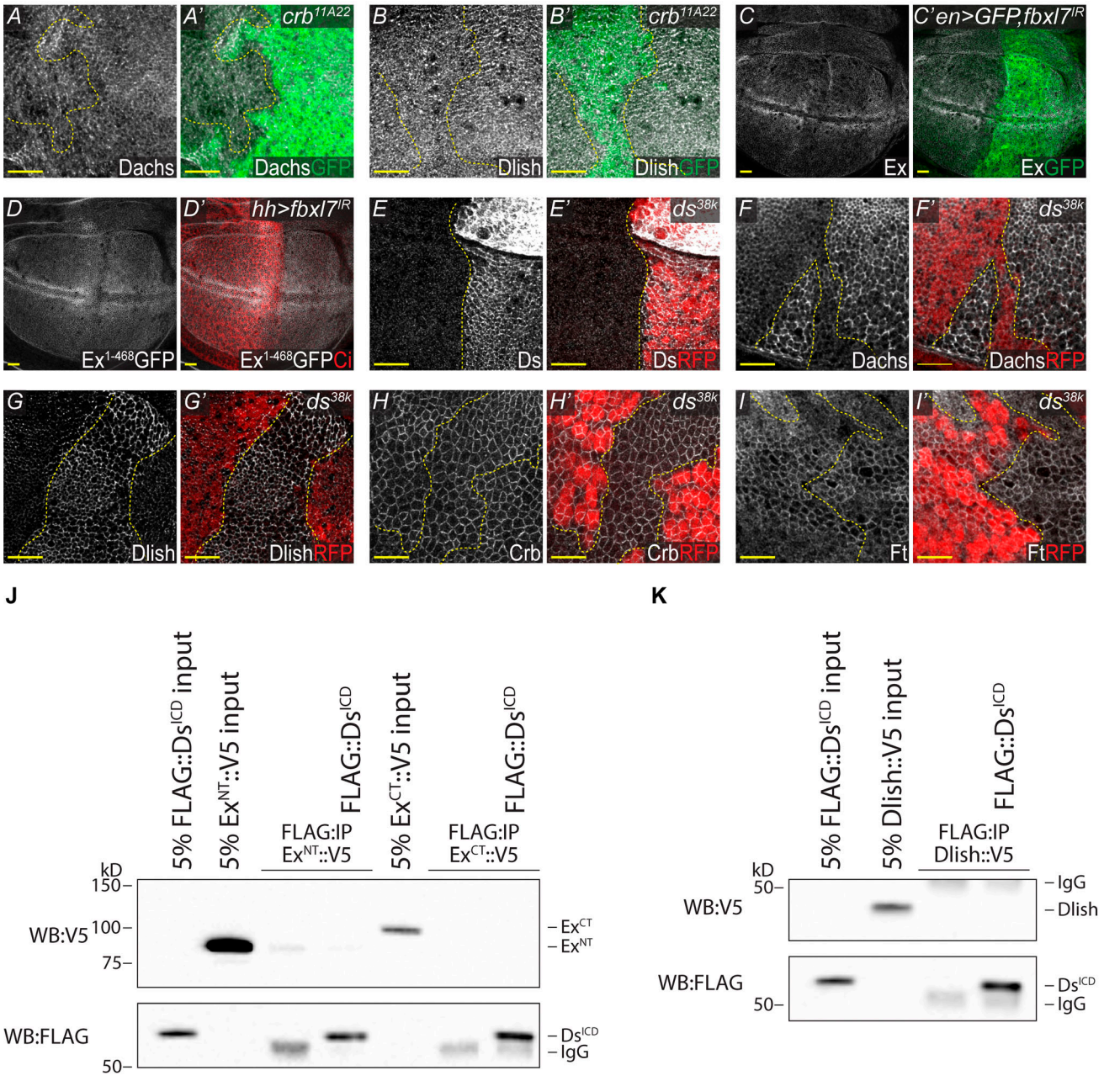

Figure S5. **Analysis of *crh*, *fbxl7*, and *ds* phenotypes and Ds binding. (A–B′)** Loss of Crb has no effect on Dachs and Dlish. XY confocal micrographs of third instar wing imaginal discs containing crb11A22 mutant clones (marked by absence of GFP shown in green) with Dachs staining (A and A′—shown in gray) and Dlish staining (B and B′—shown in gray). **(C and C′)** RNAi-mediated knockdown of Fbxl7 has no effect on Ex. XY confocal micrographs of third instar wing imaginal discs where en-Gal4 was used to drive expression of *UAS-Dicer2,UAS-GFP,UAS-fbxl7^{IR}* with Ex staining (shown in gray). GFP marks the Gal4 positive posterior compartment (shown in green). **(D and D′)** RNAi-mediated knockdown of Fbxl7 has no effect on ubi-Ex1-468::GFP. XY confocal micrographs of third instar wing imaginal discs where *hh-Gal4* was used to drive expression of *UAS-fbxl7^{IR}* with direct GFP fluorescence representing ubi-Ex$^{1\text{-}468}$::GFP (shown in gray). Cubitus Interruptus (Ci) staining marks the Gal4 negative anterior compartment (shown in red). **(E and E′)** Validation of *ds^{38k}* as a protein null. XY confocal micrographs of third instar wing imaginal discs containing *ds^{38k}* mutant clones (marked by absence of RFP shown in red) with Ds staining (shown in gray). **(F–G′)** Loss of *ds* dramatically increases apical Dachs and Dlish. XY confocal micrographs third instar wing imaginal discs containing *ds^{38k}* mutant clones (marked by absence of RFP shown in red) with Dachs staining (F and F′, shown in gray) and Dlish staining (G and G′, shown in gray). **(H and H′)** Loss of *ds* has no effect on Crb. XY confocal micrographs third instar wing imaginal discs containing *ds^{38k}* mutant clones (marked by absence of RFP shown in red) with Crb staining (shown in gray). **(I and I′)** Loss of *ds* has a minimal effect on Ft in the pouch. XY confocal micrographs third instar wing imaginal discs containing *ds^{38k}* mutant clones (marked by absence of RFP shown in red) with Ft staining (shown in gray). All XY images are orientated as dorsal up. Clonal boundaries are marked by yellow dotted lines. Scale bars are 10 µm. **(J)** Ds^{ICD} does not bind to Ex^{NT} or Ex^{CT}. In vitro transcribed and translated Ex^{NT} or Ex^{CT} were incubated alone or with in vitro transcribed and translated Ds^{ICD} and subjected to FLAG-IP. **(K)** Ds^{ICD} does not bind to Dlish. In vitro transcribed and translated Dlish was incubated alone or with in vitro transcribed and translated Ds^{ICD} and subjected to FLAG-IP. The expression and presence of proteins was analyzed by immunoblotting with the indicated antibodies. WB, Western blot. Source data are available for this figure: SourceData FS5.

Provided online is Table S1, which shows constructs made for this study.